Limited role for transforming growth factor- pathway activation-mediated escape from VEGF inhibition in murine glioma models

Mangani, D ; Weller, M ; Seyed Sadr, E ; Willscher, E ; Seystahl, K ; Reifenberger, G ; Tabatabai, G ; Binder, H ; Schneider, H

Abstract: BACKGROUND The vascular endothelial growth factor (VEGF) and transforming growth factor (TGF)- pathways regulate key biological features of glioblastoma. Here we explore whether the TGF- pathway, which promotes angiogenesis, invasiveness, and immunosuppression, acts as an escape pathway from VEGF inhibition. METHODS The role of the TGF- pathway in escape from VEGF inhibition was assessed in vitro and in vivo and by gene expression profiling in syngeneic mouse glioma models. RESULTS We found that TGF- is an upstream regulator of VEGF, whereas VEGF pathway activity does not alter the TGF- pathway in vitro. In vivo, single-agent activity was observed for the VEGF antibody B20-4.1.1 in 3 and for the TGF- receptor 1 antagonist LY2157299 in 2 of 4 models. Reduction of tumor volume and blood vessel density, but not induction of hypoxia, correlated with benefit from B20-4.1.1. Reduction of phosphorylated (p)SMAD2 by LY2157299 was seen in all models but did not predict survival. Resistance to B20 was associated with anti-angiogenesis escape pathway gene expression, whereas resistance to LY2157299 was associated with different immune response gene signatures in SMA-497 and GL-261 on transcriptomic profiling. The combination of B20 with LY2157299 was ineffective in SMA-497 but provided prolongation of survival in GL-261, associated with early suppression of pSMAD2 in tumor and host immune cells, prolonged suppression of angiogenesis, and delayed accumulation of tumor infiltrating microglia/macrophages. CONCLUSIONS Our study highlights the biological heterogeneity of murine glioma models and illustrates that cotargeting of the VEGF and TGF- pathways might lead to improved tumor control only in subsets of glioblastoma.

DOI: https://doi.org/10.1093/neuonc/now112

Limited role for transforming growth factor-β pathway activation-mediated escape from VEGF inhibition in murine glioma models

Davide Mangani[1], Michael Weller[1,2], Emad Seyed Sadr[1], Edith Willscher[3], Katharina Seystahl[1], Guido Reifenberger[4], Ghazaleh Tabatabai[1,2,*], Hans Binder[3], Hannah Schneider[1]

[1]Laboratory of Molecular Neuro-Oncology, Department of Neurology, University Hospital and University of Zurich, Zurich, Switzerland

[2]Center for Neuroscience, University of Zurich, Zurich, Switzerland

[3] Interdisciplinary Center for Bioinformatics, University of Leipzig, Leipzig, Germany

[4] Institute of Neuropathology, Heinrich Heine University, Duesseldorf, and German Cancer Consortium (DKTK), German Cancer Research Center (DKFZ) Heidelberg, partner site Essen/Duesseldorf, Germany

Running Title: TGF-β pathway as escape from VEGF inhibition in glioblastoma

Corresponding author: Michael Weller, MD, Department of Neurology, University Hospital Zurich, Zurich Switzerland, phone +41 44 2555500, fax +41 44 2554507, e-Mail michael.weller@usz.ch

*Current address: Interdisciplinary Division of Neuro-Oncology, University Hospital Tuebingen, Laboratory of Clinical and Experimental Neuro-Oncology, Hertie Institute for Clinical Brain Research, Eberhard Karls University, Tuebingen, Germany

Funding: This study was supported by a grant from Oncosuisse (KFS-02694-08-2010) to M.W. and G.T.

Conflicts of interest: M. Weller has received research grants from Roche and honoraria for lectures or advisory board participation from Lilly and Roche. K. Seystahl has received honoraria from Roche for advisory board participation. G. Reifenberger has received research grants from Roche and Merck as well as honoraria for lectures or advisory board participation from Amgen and Celldex. G. Tabatabai received research and travel grants and honoraria for lectures and Advisory board participation from Roche. The authors declare no additional competing financial interests.

Total manuscript word count: 5984

Abstract

Background. The vascular endothelial growth factor (VEGF) and transforming growth factor (TGF)-β pathways regulate key biological features of glioblastoma. Here we explored whether the TGF-β pathway which promotes angiogenesis, invasiveness and immunosuppression, acts as an escape pathway from VEGF inhibition.

Methods. The role of the TGF-β pathway in escape from VEGF inhibition was assessed *in vitro* and *in vivo* and by gene expression profiling in syngeneic mouse glioma models.

Results. We found that TGF-β is an up-stream regulator of VEGF whereas VEGF pathway activity does not alter TGF-β pathway *in vitro*. *In vivo*, single agent activity was observed for the VEGF antibody B20-4.1.1 in three, and for the TGF-β receptor I antagonist LY2157299 in two of four models. Reduction of tumor volume and blood vessel density, but not induction of hypoxia, correlated with benefit from B20-4.1.1. Reduction of pSMAD2 by LY2157299 was seen in all models, but did not predict survival. Resistance to B20 was associated with anti-angiogenesis escape-pathway-gene-expression whereas resistance to LY2157299 was associated with different immune response gene signatures in SMA-497 and GL-261 on transcriptomic profiling. The combination of B20 with LY2157299 was ineffective in SMA-497, but provided prolongation of survival in GL-261, associated with early suppression of pSMAD2 in tumor and host immune cells, prolonged suppression of angiogenesis, and delayed accumulation of tumor infiltrating microglia/macrophages.

Conclusions. Our study highlights the biological heterogeneity of murine glioma models and illustrates that co-targeting of the VEGF and TGF-β pathways might lead to improved tumor control only in subsets of glioblastoma.

Keywords: Glioblastoma; VEGF; TGF-β; coinhibition; escape mechanism

Introduction

Glioblastoma remains a universally fatal neoplasm despite some advances in its multidisciplinary management, e.g., the introduction of combined modality treatment including post-surgical radiotherapy with concomitant and maintenance temozolomide (TMZ/RT→TMZ) [1,2]. Several current strategies of glioblastoma treatment focus on the inhibition of angiogenesis, largely the VEGF pathway . Yet, the lead compound bevacizumab has not been approved in Europe for treatment of recurrent glioblastoma because an effect on overall survival has not been demonstrated, and the recently completed EORTC 26101 trial failed to demonstrate superior survival with the combination of bevacizumab with lomustine over lomustine alone [3]. Further, two phase III trials in the newly diagnosed setting achieved prolonged progression-free survival, but not overall survival [4,5]. While the potential clinical benefit of improving progression-free survival is not disputed, these study results call for combination therapies of VEGF antagonism with other targeted agents that may extend progression-free survival further and allow to confer a survival benefit.

One likely explanation for the failure of VEGF antagonism to prolong overall survival is the induction of a biological change in tumors that eventually fail bevacizumab and then seem to be rather refractory to all further treatments. While it has been claimed that VEGF antagonism induces a more infiltrative phenotype in animal models [6], this assumption has been confirmed neither in retrospective analyses of recurrent glioblastoma patients [7] nor in the AVAglio trial[8].

TGF-β is a multifunctional cytokine implicated in the pathogenesis of glioblastoma, based on immunosuppressive properties and promotion of migration, invasion, angiogenesis and stem cell maintenance [9]. Therapeutic activity of TGF-β antagonism has been demonstrated in animal models of glioma, but translation of TGF-β antagonism into the clinic has remained

challenging. The most advanced TGF-β antagonist is the receptor kinase inhibitor, LY2157299 [10,11], which is currently explored in newly diagnosed and recurrent glioblastoma . There are multiple potential interdependencies between angiogenesis and the TGF-β pathway. Importantly, TGF-β has been identified as a positive up-stream regulator of VEGF mRNA expression and release and angiogenesis in cancer and non-neoplastic cells [12-16], providing a strong rationale for combining TGF-β and VEGF inhibition. Accordingly, we here explored the crosstalk between these pathways in syngeneic murine glioma models and asked whether co-targeting the VEGF and TGF-β pathways provides a new perspective for the treatment of glioblastoma.

Materials and methods

Reagents

Recombinant human TGF-β_2 was purchased from R&D systems (Minneapolis, MN) and murine VEGF ($VEGF_{120}$) from biolegend (San Diego, CA). B20-4.1.1 (B20) was kindly provided by T. R. Schwartz (Genentech, South San Francisco, CA), cediranib by AstraZeneca (London, UK) and LY2157299 (LY) by Eli Lilly & Co. (Indianapolis, MN).

Cell lines

Murine SMA-497, SMA-540 and SMA-560 glioma cells were kindly provided by D.D. Bigner (Durham, NC). GL-261 cells were received from the National Cancer Institute (Frederick, MD).

Viability and clonogenicity assays

Viability was assessed after pooling adherent and floating cells by trypan blue dye exclusion. Clonogenicity was assessed as previously described [17]. Cells were treated with either LY2157299 (Eli Lilly & Co. 1μM), cediranib (AstraZeneca, 100 nM) or B20 (Genentech, 100 μg/ml)..

Real-time PCR (RT-PCR)

Total mRNA for gene expression analyses was extracted from murine glioma cells after 24 h incubation in serum-free medium (SFM) or from *in vivo* tumor tissue[13]. For RT-PCR, gene expression was measured using the Real Time PCR System 7300 (Applied Biosystems, Foster City, CA) with SYBR Green Master Mix (AppliChem, Darmstadt, Germany) and primers at optimized concentrations.

Immunoblot analyses

For immunoblot analysis, whole cell lysates were prepared, proteins were separated under denaturating conditions following blotting and antibody detection.

Enzyme-linked immunosorbent assay (ELISA)

Supernatants from subconfluent glioma cell cultures (treated or untreated) were analysed.

Animal studies

The care and treatment of all animals was in accordance with the Swiss Federal Law on the Protection of Animals, the Swiss Federal Ordinance on the Protection of Animals and the guidelines of the Swiss confederation (permission number 38/2012). For intracranial tumor cell implantation, 2 μl of a single cell suspension in PBS were injected (1 μl/min) into the

right striatum. 5,000 SMA or 20,000 GL-261 cells were implanted in VM/Dk or C57Bl/6 mice, respectively (n=10 per group).

Immunohistochemical analysis

Cryosections were fixed, blocked and stained with primary, followed by secondary antibodies. Subsequently, quantification of immunohistological stainings was performed.

Immunofluorescence microscopy

Immunofluorescence studies were carried out on cryosections of tumor-bearing mouse brains and data analysis was performed with Bitplane Imaris (Bitplane) software [18].

Analysis of gene expression data

The generation of the microarray analysed herein has been described [19].

Statistical analyses

All *in vitro* data are representative of experiments performed in three independent experiments with similar results. All statistical analyses were performed using Prism 5 (GraphPad Software, La Jolla, CA).

For additional methods, please see Supplementary Information.

Results

Characterization of VEGF and TGF-β$_{1/2}$ ligand/receptor expression in mouse glioma cells

VEGF-A (*VEGF*) mRNA was constitutively expressed by all cell lines, with the highest levels in GL-261 and SMA-560. In contrast, the highest levels of protein release were observed in SMA-540 and SMA-560 (Fig. 1A). VEGF receptor (*VEGFR*)*1* mRNA was expressed in all cell lines and protein levels correlated well, with highest levels in SMA-560. SMA-560 showed the highest *VEGFR2* mRNA levels followed by SMA-540, and protein was only detected in SMA-540 and SMA-560 (Fig. 1B). We also examined *ex vivo* tumoral mRNA expression of ligands and receptors, using syngeneic normal brain tissue (NBT) of VM/Dk and C57BL/6 mice as a reference. *In vitro* maintained monolayer cultures (MC) and mouse gliomas *in vivo* (T) showed similar *VEGF* mRNA levels (Fig. S1A). Compared with MC, there were higher *VEGFR1* mRNA in SMA-497 and GL-261, and higher *VEGFR2* mRNA levels in all models *in vivo* (Fig. S1B,C), suggesting a major contribution from tumor blood vessels or up-regulation of expression in tumor cells *in vivo*. Immunohistochemical stainings of VEGFR2 levels revealed a major contribution from tumor cells, even masking a typical vessel staining pattern, which, however, became readily visible in tumors stained for CD31 (see below) (Fig. S1D,E).

TGF-β$_{1/2}$ mRNA was abundant in all four models. There was no apparent correlation between mRNA and protein levels, and TGF-β$_1$ consistently exceeded TGF-β$_2$ protein levels in the supernatant. TGF-β receptor 2 (*TGFβR2*) and activin receptor-like kinase 5 (*ALK-5*) were expressed in all models at variable levels, with correlation between mRNA and protein (Fig. 1C,D). *TGF-β$_1$* but not *TGF-β$_2$* mRNA was enhanced *in vivo* in SMA-497, SMA-560 and GL-261. While *ALK-5* mRNA was consistently increased *in vivo*, there was a mixed pattern for

TGFβR2 mRNA expression with increased expression in SMA-560, and a trend for decreased expression in the other models (Fig. S1F-I).

Modulation and consequences of VEGF and TGF-$\beta_{1/2}$ signaling in vitro

We observed an increase in pVEGFR1 levels in response to exogenous VEGF in SMA but not in GL-261 glioma cells. pVEGFR2 was increased upon VEGF stimulation in SMA-540 and SMA-560 (Fig. S2A). An increase in pSMAD2 was observed in all models after exposure to exogenous TGF-β_2. LY2157299 attenuated constitutive and induced SMAD2 phosphorylation (Fig. S2B). Neither VEGF pathway inhibition using B20 nor relevant concentrations of cediranib nor TGFβ pathway inhibition by LY2157299 affected viability or clonogenicity (Fig. S2D,E).

Murinized bevacizumab prolongs survival in SMA-540, SMA-560 and GL-261 glioma models

We next determined single agent activity of B20 treatment in the four mouse glioma models. Histological analyses of tumors harvested when the first clinical symptoms occurred (early-stage) revealed reduced tumor volumes in all models except SMA-497. Tumor volume reduction was not paralleled by changes in Ki-67 labeling (Fig. 2A,B). Solvent-treated tumors possessed well-delineated margins whereas tumor borders in the B20 treatment groups were frayed and surrounded by numerous smaller satellites in all models (Fig. S3A,B). The number of intratumoral vessels was decreased in SMA-540, SMA-560 and GL-261, but not in SMA-497 (Fig. 2C, Fig. S3C). Vessel morphology was specifically changed in GL-261 with decreased vessel diameter. CA IX staining as a surrogate marker for hypoxia was strongly induced in SMA-540 and SMA-560, but still not reaching constitutive levels of the SMA-497 model (Fig. 2D, Fig. S3D). In general, CA IX staining was inversely related to CD31 labeling, confirming that hypoxia develops with increasing distance from blood vessels (Fig. S3F).

Finally, B20 prolonged survival in the SMA-540, SMA-560 and GL-261 models, but not in SMA-497 (Fig. 2F, Table S1). Our hypothesis of induced activation of the TGF-β pathway as an escape route from VEGF inhibition led us to predict increased pSMAD2 levels in B20-treated tumors at least at progression. However, we observed decreased pSMAD2 levels in 2 of 4 mouse models *in vivo,* and no change in the other two models, in fact, there was an association between decreased pSMAD2 levels and benefit from B20 (Fig. 2E, Fig. S3E). This decrease in pSMAD2 levels was observed in tumor cells and tumor-infiltrating leukocytes. Tumor cells were more frequently pSMAD2-positive than host cells indicating that tumor cells may be more responsive to TGF-β than host cells (Fig. S3G). Further, we noted that, in sharp contrast to the initial hypothesis of B20-triggered hypoxia followed by hypoxia-induced, TGF-β-mediated, invasiveness, induction of hypoxia and reduction of pSMAD2 were seen in the same models. Accordingly, all four cell lines responded to hypoxia with decreased pSMAD2 levels *in vitro*, too (Fig. S2C). Bioinformatic analyses of previously published data [19] focusing on angiogenesis gene sets (Table S2) revealed that SMA-497 express high levels of genes involved in angiogenic escape pathways (Fig. 2G, Table S3). Unsupervised clustering of significantly regulated genes further revealed that genes up-regulated in SMA-497 were mainly down-regulated in GL-261, and *vice versa* (Figure 2G, encircled clusters). Further assessment of these gene clusters by STRING analysis visualized the differential activation or down-regulation of genes of the angiogenic genesets in SMA-497 and GL-261 (Fig. S3H,I).

LY2157299 prolongs survival in SMA-560 and SMA-540 murine glioma models

Next we determined single agent activity of LY2157299 in the four mouse glioma models. Histological analyses of tumors harvested when the first clinical symptoms occurred revealed a trend towards reduced tumor volumes only in SMA-560 (Fig. 3A, Fig. S4A). We then explored whether exposure to LY2157299 suppressed pSMAD2 as a surrogate marker of

TGF-β pathway activity. pSMAD2 levels were decreased by LY2157299 in all models (Fig. 3B, Fig. S4B, left), confirmed by immunoblot in SMA-560 (Fig. S4B, right). Intratumoral vessel density was unaffected in either model but vessel morphology was changed in all models, except SMA-497, towards a vasculature with decreased vessel diameter and lumina upon LY2157299 treatment (Fig. 3C, Fig. S4C). LY2157299 prolonged survival in SMA-560 and SMA-540, but not SMA-497 or GL-261 (Fig. 3D, Table S1). Accordingly, transcriptomic analysis of TGF-β receptor signaling pathway gene sets (Table S4) showed SMA-540 and SMA-560 to be the cell lines with the highest TGF-β pathway activity (Fig. 3E, Table S5). The survival differences in the SMA-540 control groups in the studies reported in Figures 2 and 3 is explained by variations in the tumorigenicity in this model which is the least tumorigenic. Transcriptomic profiling also revealed that the most immunogenic tumors as defined by Gene Ontology, SMA-497 and GL-261, exhibited differential clusters of up- and down-regulated genes involved in immune response pathways. Genes up-regulated in SMA-497 were mainly down-regulated in GL-261, and *vice versa* (Fig. 3F encircled, Table S6,7). STRING analysis of the differentially regulated gene clusters visualized the differential activation or down-regulation of genes of the immune response-related gene sets in SMA-497 and GL-261 (Fig. S4D,E).

Reciprocal modulation of the VEGF and TGF-β pathway in vitro

We next assessed the expression of ligands and receptors of the VEGF and TGF-β pathways in the mouse glioma models after reciprocal stimulation. First we explored whether modulation of VEGF signaling in glioma cells affected the TGF-β pathway. Exposure to exogenous VEGF, B20 or cediranib had no effect on TGF-$\beta_{1/2}$ mRNA and protein levels (Fig. S5A,B) or pSMAD2 levels (Fig. S5C). Conversely, VEGF mRNA expression and protein release were induced by TGF-β_2 in a LY2157299-sensitive manner. VEGF mRNA expression was also increased in all cells in response to hypoxia whereas protein levels were increased in

SMA-497, SMA-540 and GL-261 and remained similar in SMA-560 (Fig. S5D,E). Furthermore, we observed an increase in total *VEGFR1* mRNA expression in response to TGF-β_2 in SMA-497 and SMA-560 glioma cells which was decreased upon co-treatment with LY2157299 only in SMA-560. However, protein levels were increased in all models and this effect was blocked by LY2157299 (Fig. S5F). VEGFR2 levels in response to TGF-β_2 stimulation, analyzed in SMA-540 and SMA-560 cells only, were increased upon stimulation in a LY2157299-sensitive manner (Fig. S5G). Although LY2157299 alone reduced constitutive pSMAD2 levels (Fig. S2B), it had no effect on constitutive VEGF ligand or receptor mRNA expression or protein release in either cell line.

Co-targeting of the VEGF and TGF-β pathways in vivo

SMA-497 and GL-261 were chosen to explore a potential synergy between VEGF and TGF-β pathway inhibition. SMA-497 was chosen because it was refractory to either treatment as single agent, facilitating the detection of any possible synergy. GL-261 was chosen because LY2157299 alone was not active whereas B20 was. A gain from co-treatment would indicate that the TGF-β pathway assumes a different role in the context of VEGF inhibition. There was no survival benefit from co-treatment in SMA-497 whereas combination treatment was superior to either treatment alone in GL-261 (Fig. 4A-E, Table S1). Early reductions of tumor volumes and blood vessel density were seen in GL-261, but not SMA-497, and only in the B20-containing regimens, with no modulation by LY2157299. The volume differences in early-stage GL-261 tumors were abolished in end-stage tumors. However, reduced blood vessel density was only maintained in the co-treatment group, but not in the B20-only end-stage tumors (Fig. 4A,B). Decreased vessel diameter and increased vessel wall thickness were observed with all therapeutic regimens in GL-261 (Fig. S6B,F). ZO-1 was used as a marker for tight junction staining showing a more regular staining pattern indicative for a restoration of endothelial barrier integrity (Fig. S6I-L). Co-treatment with LY2157299 prevented B20-

induced increased tumor invasiveness in early stages, but this effect was abolished in end-stage tumors (Fig. S6A,E). In GL-261, but not SMA-497 gliomas, the reduction of pSMAD2 levels by LY2157299 alone was enhanced by co-treatment with B20 in early-stage responsive and in end-stage resistant tumors. In contrast, pSMAD2 levels were increased in B20-treated end-stage tumors, consistent with the TGF-β pathway as an escape route from VEGF inhibition, and this was not seen with combined treatment (Fig. 4C, Fig. S6C,G). There was no significant CA IX induction in either model in early-stage tumors whereas treatment resistance in the GL-261 co-treatment group was accompanied by an increase in CA IX staining from 18% to 39% positive tumor areas (Fig. 4D, Fig. S6D,H). Assessment of the role of TGF-$\beta_{1/2}$ within angiogenesis gene clusters up-regulated in SMA-497 and GL-261 by STRING analysis revealed that TGF-$\beta_{1/2}$ interact with only a small subset of up-regulated genes in SMA-497. Conversely, both molecules are integrated in the main network of functional gene interactions in GL-261 (Fig. 4F), indicating a possible role of TGF-β in mediating resistance to B20 therapy.

Differential host cell responses to VEGF/TGF-β co-targeting

To generate a broad overview on host cell infiltration, we assessed frequencies of leukocytes (CD45+), T cells (CD4+ and CD8+) and macrophages/microglia (CD11b+)in mono- and co-treated SMA-497 and GL-261 early- and end-stage tumors (Fig. 5A-D, Fig. S7A-H). In GL-261, only in early- but not in end-stage tumors, increased infiltration of CD11b+ cells upon B20 alone and increased numbers of cytotoxic T (CD8+) cells upon co-treatment were observed (Fig. 5C,D, Fig. S7C,D). Resistance to co-treatment was accompanied by decreased infiltration of CD45+ and CD11b+ cells in GL-261 end-stage gliomas when compared to solvent or B20 mono-treatment (Fig. 5A,D, Fig. S7E,H).

pSMAD2 was detected in tumor cells rather than host leukocytes in GL-261 end-stage tumors. Due to the higher proportion of pSMAD2-positive tumor cells versus infiltrating

leukocytes, tumor cells were more affected by decreased pSMAD2 levels, although levels in single leukocytes were altered similarly, with a decrease upon LY2157299 and combined treatment, and an increase by B20 alone (Fig. 6A-D).

pSMAD2 levels in response to bevacizumab treatment in human glioblastoma

We also analysed human glioblastoma patients who underwent further surgery upon failure of bevacizumab. As groups, neither refractory tumors of 9 non-bevacizumab-treated patients, nor those of 5 patients failing on a bevacizumab-containing regimen, exhibited an increase or decrease in pSMAD2 levels whereas vessel density was decreased in the latter group (Fig. S8A-F).

Discussion

Interactions between human tumors and their specific microenvironment determine growth characteristics and responses to radiotherapy or pharmacotherapy [20]. This notion is particularly true for glioblastoma which typically contains major host cell infiltrates which probably support rather than limit tumor growth [21-23].

Here we focused on two cytokine-dependent signaling pathways attributed a major role in the pathogenesis of glioblastoma, VEGF and TGF-β, using a panel of syngeneic mouse gliomas as model systems [19]. Responsiveness to VEGF and TGF-β stimulation as assessed by VEGFR and SMAD2 phosphorylation as well as a positive regulation of VEGF by TGF-β, but not vice versa, was confirmed *in vitro* ((Fig. 1, Fig. S1,S2,S5). Inhibition of neither pathway has prominent effects on glioma cell viability or growth *in vitro* (Fig. S2) although growth suppressive properties have been reported for TGF-β_1 in the SMA-560 model [24].

There was differential responsiveness to B20-mediated VEGF inhibition alone. While high expression of VEGF and VEGFR is consistent with responsiveness of SMA-560, the

responsiveness of SMA-540 was less well explained, and the expression levels of VEGF in GL-261 did not translate into superior efficacy of B20. The responsiveness of GL-261 despite unaltered proliferation and hypoxia is consistent with direct induction of cell death by VEGF inhibition in some mouse glioma models [25,26]. A high constitutive level of hypoxia and failure to reduce blood vessel density in response to B20, consistent with VEGF-independent angiogenesis, were prominent features of the refractory SMA-497 model. Of note, full suppression of angiogenesis was not achieved in any model (Fig. 2 and Fig. S3). Although all SMA lines were derived from one tumor, they exhibited major variation in response to different treatment settings that were tentatively linked to differential transcriptomics specifically among angiogenesis-related gene sets (Fig. 2, Tables S2,S3).

The TGF-βR1 inhibitor LY2157299 was active pharmacodynamically as assessed by a decrease of pSMAD2 levels *in vivo*, although no full suppression was achieved, indicating either insufficient pharmacodynamic properties and target coverage, or ALK-5-independent pathways maintaining pSMAD2 phosphorylation, or both (Fig. 3 and Fig. S4). The two models responsive to LY2157299 *in vivo*, SMA-540 and SMA-560, exhibited increased expression levels of genes of the TGF-β receptor signaling pathway (Fig. 3). Similar to anti-angiogenic therapy, also TGF-β antagonism has been linked to vascular normalization and improved drug delivery [27]. Accordingly, we observed morphological changes related to vascular normalization in tumor vessels upon LY2157299 treatment in all models, consisting of increased vessel wall thickness and decreased vessel diameter (Fig. 3C, Fig. S4C). It is tempting to link these uniform changes in blood vessel morphology, induced by LY2157299, to the effects of TGF-β on VEGF and VEGFR expression *in vitro* (Fig. S4,5). A transcriptional profiling study of human glioblastoma vessels indicated key roles in the process of pathological angiogenesis for *VEGF-A* and *TGF-β2* [28]. The decrease in pSMAD2 levels in response to hypoxia *in vitro* and to hypoxia in association with B20 treatment *in vivo* in two of three responsive models was surprising (Fig. 2, Fig. S2) since no evidence suggests

that the TGF-β pathway is negatively regulated by hypoxia. Interestingly, pSMAD2 levels positively correlated with tumor proliferation in human glioblastoma [9]. Accordingly, we also found parallel changes in the levels of both markers (Fig. 2, Fig. S2).

VEGFR inhibition *in vitro* did not decrease pSMAD2 levels in any cell line (Fig. S5). Yet, the synergistic suppression of pSMAD2 levels by B20 and LY2157299 co-treatment in early-stage tumors and increased pSMAD2 levels in end-stage tumors with B20 treatment alone are consistent with the hypothesis that enhanced TGF-β activity might promote eventual escape from VEGF inhibition at least in the GL-261 model. Immunohistochemical analysis of orthotopic U87MG gliomas had indeed revealed increased TGF-β protein levels upon anti-VEGF treatment, too [29].

Increased levels of CD11b-positive macrophages/microglia have been linked to refractoriness to anti-VEGF treatment [30] and attributed a role in the VEGF-independent restoration of tumor vessels by vasculogenic, but not angiogenic processes [31]. Supporting this concept, we observed that co-targeting VEGF and TGF-βR1 decreased the numbers of intratumoral CD11b+ cells and that tumors failed to re-vascularize compared to B20 alone in GL-261 end-stage tumors (Fig. 5 and Fig. S6,7). Similarly, coinhibition of VEGF and the angiopoietin-2 pathway provided improved tumor control and reduced numbers of F4/80-positive macrophages in the GL-261 model [25]. Possibly, targeting TGF-β alters CD11b+ cell recruitment via interacting with the CXCR4-CXCL12 axis since VEGFR inhibitors can up-regulate chemokine (C-X-C motif) receptor 4 (CXCR4) in glioblastoma cells by a TGF-β-dependent mechanism [32] and since TGF-β up-regulates CXCR4 expression in monocytes, macrophages, T naïve cells and other immune cell populations [33,34].

Altogether, according to our analysis in the GL-261 model, the tumor-promoting role of TGF-β would relate more to facilitating angiogenesis or vasculogenesis than to promote a more invasive phenotype even when combined with VEGF antagonists. This is because B20-treated tumors were more invasive early on when pSMAD2 levels were still low and because co-

treatment with LY2157299 still suppressed tumor vasculature in end-stage disease (Fig. 2,4). Yet, B20-induced hypoxia may ultimately promote lactate dehydrogenase activity [35] which in turn may stimulate TGF-β signaling associated with an angiogenic signaling [36].

Unexpectedly, we observed that mainly tumor cells but not leukocytes exhibited phosphorylated SMAD2 (Fig. 6 and Fig. S3). Previous studies have already indicated that pSMAD2 levels are high in glioblastoma cells, indicating that tumor cells do not have to escape TGF-β signaling at least at the level of SMAD2 phosphorylation [9,37]. However, pSMAD2 levels in B20-treated GL-261 end-stage tumors increased proportionally in tumor cells and leukocytes (Figure 6). Since the activation of TGF-β signaling in tumors has been linked to immunosuppression [38], increased pSMAD2 levels indicate a TGF-β-induced immunosuppressive tumor micromilieu during anti-VEGF treatment which might be an important factor of therapy failure. Yet, preliminary studies in paired human glioblastoma samples provided no evidence for enhanced pSMAD2 levels at recurrence, either without or with previous bevacizumab therapy (Fig. S8).

Limitations of the present study include the challenges in determining volumes of infiltrative rodent gliomas, the restriction to mouse models based on long-term cell lines, and the exploration of co-treatment rather than sequential treatments. Moreover, we did not distinguish B20 or LY2157299 effects on tumor versus host cells and effects of B20 on VEGFR1 versus VEGFR2 signaling in mouse glioma cells [39], and the human patient cohort was small.

Our study highlights the relevance of hypoxia in the malignant phenotype of glioblastoma and its resistance to therapy. SMA-497 showed the highest constitutive level of hypoxia and was refractory to all therapeutic interventions. GL-261 eventually became hypoxic when escaping combination therapy (Fig. 4 and Fig. S6). We conclude that at least for subsets of glioblastomas, co-targeting of VEGF and TGF-β pathways might result in a permanent vascularization deficiency which results in prolonged tumor control. Ultimately, however,

such microenvironment-targeting therapies may only be successful if combined with pharmacological or cell-based therapies that exert relevant tumor cell cytotoxicity, since the major cell biological changes observed in selected models did not translate into major gains in survival

Funding: This study was supported by a grant from Oncosuisse (KFS-02694-08-2010) to M.W. and G.T.

Acknowledgments: We thank Michael Lahn (Eli Lilly & Co., Indianapolis, MN) for valuable discussions.

References

1. Weller M, van den Bent M, Hopkins K, et al. EANO guideline for the diagnosis and treatment of anaplastic gliomas and glioblastoma. *The lancet oncology.* 2014; 15(9):e395-403.

2. Weller M, Wick W, Aldape K, et al. Glioma. *Nature Reviews Disease Primers.* 2015:15017.

3. Wick W, Brandes A, Gorlia T, et al. LB-05Phase III Trial Exploring The Combination Of Bevacizumab And Lomustine In Patients With First Recurrence Of A Glioblastoma: The EORTC 26101 Trial. *Neuro-oncology.* 2015; 17(suppl 5):v1.

4. Chinot OL, Wick W, Mason W, et al. Bevacizumab plus radiotherapy-temozolomide for newly diagnosed glioblastoma. *The New England journal of medicine.* 2014; 370(8):709-722.

5. Gilbert MR, Dignam JJ, Armstrong TS, et al. A randomized trial of bevacizumab for newly diagnosed glioblastoma. *The New England journal of medicine.* 2014; 370(8):699-708.

6. Paez-Ribes M, Allen E, Hudock J, et al. Antiangiogenic therapy elicits malignant progression of tumors to increased local invasion and distant metastasis. *Cancer cell.* 2009; 15(3):220-231.

7. Wick A, Dorner N, Schafer N, et al. Bevacizumab does not increase the risk of remote relapse in malignant glioma. *Annals of neurology.* 2011; 69(3):586-592.

8. Wick W, Cloughesy TF, Nishikawa R, et al. Tumor response based on adapted Macdonald criteria and assessment of pseudoprogression (PsPD) in the phase III AV Aglio trial of bevacizumab (Bv) plus temozolomide (T) plus radiotherapy (RT) in newly diagnosed glioblastoma (GBM). *Journal of Clinical Oncology.* 2013; 31(15).

9. Bruna A, Darken RS, Rojo F, et al. High TGFbeta-Smad activity confers poor prognosis in glioma patients and promotes cell proliferation depending on the methylation of the PDGF-B gene. *Cancer cell.* 2007; 11(2):147-160.

10. Rodon J, Carducci MA, Sepulveda-Sanchez JM, et al. First-in-human dose study of the novel transforming growth factor-beta receptor I kinase inhibitor LY2157299 monohydrate in patients with advanced cancer and glioma. *Clinical cancer research : an official journal of the American Association for Cancer Research.* 2015; 21(3):553-560.

11. Herbertz S, Sawyer JS, Stauber AJ, et al. Clinical development of galunisertib (LY2157299 monohydrate), a small molecule inhibitor of transforming growth factor-beta signaling pathway. *Drug Des Devel Ther.* 2015; 9:4479-4499.

12. Hjelmeland MD, Hjelmeland AB, Sathornsumetee S, et al. SB-431542, a small molecule transforming growth factor-beta-receptor antagonist, inhibits human glioma

cell line proliferation and motility. *Molecular cancer therapeutics.* 2004; 3(6):737-745.

13. Seystahl K, Tritschler I, Szabo E, Tabatabai G, Weller M. Differential regulation of TGF-beta-induced, ALK-5-mediated VEGF release by SMAD2/3 versus SMAD1/5/8 signaling in glioblastoma. *Neuro-oncology.* 2015; 17(2):254-265.

14. Pertovaara L, Kaipainen A, Mustonen T, et al. Vascular endothelial growth factor is induced in response to transforming growth factor-beta in fibroblastic and epithelial cells. *The Journal of biological chemistry.* 1994; 269(9):6271-6274.

15. Pepper MS, Vassalli JD, Orci L, Montesano R. Biphasic effect of transforming growth factor-beta 1 on in vitro angiogenesis. *Experimental cell research.* 1993; 204(2):356-363.

16. Pepper MS. Transforming growth factor-beta: vasculogenesis, angiogenesis, and vessel wall integrity. *Cytokine & growth factor reviews.* 1997; 8(1):21-43.

17. Happold C, Roth P, Silginer M, et al. Interferon-beta induces loss of spherogenicity and overcomes therapy resistance of glioblastoma stem cells. *Molecular cancer therapeutics.* 2014; 13(4):948-961.

18. Roth P, Silginer M, Goodman SL, et al. Integrin control of the transforming growth factor-beta pathway in glioblastoma. *Brain : a journal of neurology.* 2013; 136(Pt 2):564-576.

19. Ahmad M, Frei K, Willscher E, et al. How stemlike are sphere cultures from long-term cancer cell lines? Lessons from mouse glioma models. *Journal of neuropathology and experimental neurology.* 2014; 73(11):1062-1077.

20. Hanahan D, Weinberg RA. Hallmarks of cancer: the next generation. *Cell.* 2011; 144(5):646-674.

21. Murdoch C, Muthana M, Coffelt SB, Lewis CE. The role of myeloid cells in the promotion of tumour angiogenesis. *Nature reviews. Cancer.* 2008; 8(8):618-631.

22. Maes W, Verschuere T, Van Hoylandt A, Boon L, Van Gool S. Depletion of regulatory T cells in a mouse experimental glioma model through anti-CD25 treatment results in the infiltration of non-immunosuppressive myeloid cells in the brain. *Clinical & developmental immunology.* 2013; 2013:952469.

23. Vom Berg J, Vrohlings M, Haller S, et al. Intratumoral IL-12 combined with CTLA-4 blockade elicits T cell-mediated glioma rejection. *The Journal of experimental medicine.* 2013; 210(13):2803-2811.

24. Ashley DM, Sampson JH, Archer GE, Hale LP, Bigner DD. Local production of TGF beta1 inhibits cerebral edema, enhances TNF-alpha induced apoptosis and improves survival in a murine glioma model. *Journal of neuroimmunology.* 1998; 86(1):46-52.

25. Scholz A, Harter PN, Cremer S, et al. Endothelial cell-derived angiopoietin-2 is a therapeutic target in treatment-naive and bevacizumab-resistant glioblastoma. *EMBO Mol Med.* 2015; 8(1):39-57.

26. Pitter KL, Tamagno I, Alikhanyan K, et al. Corticosteroids compromise survival in glioblastoma. *Brain : a journal of neurology.* 2016; In press.

27. Liu J, Liao S, Diop-Frimpong B, et al. TGF-beta blockade improves the distribution and efficacy of therapeutics in breast carcinoma by normalizing the tumor stroma. *Proceedings of the National Academy of Sciences of the United States of America.* 2012; 109(41):16618-16623.

28. Dieterich LC, Mellberg S, Langenkamp E, et al. Transcriptional profiling of human glioblastoma vessels indicates a key role of VEGF-A and TGFbeta2 in vascular abnormalization. *J Pathol.* 2012; 228(3):378-390.

29. Piao Y, Liang J, Holmes L, et al. Glioblastoma resistance to anti-VEGF therapy is associated with myeloid cell infiltration, stem cell accumulation, and a mesenchymal phenotype. *Neuro-oncology.* 2012; 14(11):1379-1392.

30. Shojaei F, Wu X, Malik AK, et al. Tumor refractoriness to anti-VEGF treatment is mediated by CD11b+Gr1+ myeloid cells. *Nature biotechnology.* 2007; 25(8):911-920.

31. Kioi M, Vogel H, Schultz G, Hoffman RM, Harsh GR, Brown JM. Inhibition of vasculogenesis, but not angiogenesis, prevents the recurrence of glioblastoma after irradiation in mice. *The Journal of clinical investigation.* 2010; 120(3):694-705.

32. Pham K, Luo D, Siemann DW, et al. VEGFR inhibitors upregulate CXCR4 in VEGF receptor-expressing glioblastoma in a TGFbetaR signaling-dependent manner. *Cancer letters.* 2015; 360(1):60-67.

33. Wang J, Guan E, Roderiquez G, Calvert V, Alvarez R, Norcross MA. Role of tyrosine phosphorylation in ligand-independent sequestration of CXCR4 in human primary monocytes-macrophages. *The Journal of biological chemistry.* 2001; 276(52):49236-49243.

34. Franitza S, Kollet O, Brill A, et al. TGF-beta1 enhances SDF-1alpha-induced chemotaxis and homing of naive T cells by up-regulating CXCR4 expression and downstream cytoskeletal effector molecules. *European journal of immunology.* 2002; 32(1):193-202.

35. Fack F, Espedal H, Keunen O, et al. Bevacizumab treatment induces metabolic adaptation toward anaerobic metabolism in glioblastomas. *Acta neuropathologica.* 2015; 129(1):115-131.

36. Baumann F, Leukel P, Doerfelt A, et al. Lactate promotes glioma migration by TGF-beta2-dependent regulation of matrix metalloproteinase-2. *Neuro-oncology.* 2009; 11(4):368-380.

37. Frei K, Gramatzki D, Tritschler I, et al. Transforming growth factor-beta pathway activity in glioblastoma. *Oncotarget.* 2015; 6(8):5963-5977.

38. Rich JN. The role of transforming growth factor-beta in primary brain tumors. *Frontiers in bioscience : a journal and virtual library.* 2003; 8:e245-260.

39. Szabo E, Schneider H, Seystahl K, et al. Autocrine VEGFR1 and VEGFR2 signaling promotes survival in human glioblastoma models in vitro and in vivo. *Neuro-oncology.* 2016; In press.

Figure legends

Fig. 1 Expression of VEGF and TGF-β pathway ligands and receptors in mouse glioma models in vitro. SMA-497, SMA-540, SMA-560 and GL-261 cells were studied for gene expression. A, VEGF expression determined by RT-PCR for mRNA (top) and by ELISA for protein in the supernatant (bottom) *in vitro*. B, VEGFR1,2 expression determined by RT-PCR (top) and immunoblot (bottom) *in vitro*. C, TGF-β1/2 expression determined by RT-PCR (top) and ELISA in the supernatant (bottom) *in vitro*. D, TGF-βR2 and ALK-5 expression determined by RT-PCR (top) and immunoblot (bottom) *in vitro*. Values of densitometric analysis relative to β-actin are shown below the immunoblot panels in B and D.

Fig. 2 Differential effects of murinized bevacizumab on angiogenesis and growth of murine gliomas. Syngeneic mice intracranially implanted with SMA-497, SMA-540, SMA-560 or GL-261 cells were treated twice weekly with 5 mg/kg B20 or PBS from day 7 on. Brain sections (early-stage) were analysed. A, Tumor volumes. B, Ki-67 . C, CD31+ capillaries D, CA IX+ areas. E, pSMAD2. Data are expressed as mean and SEM (*$p<0.05$, **$p<0.01$, ****$p<0.0001$, unpaired student t-test, B20 versus solvent). F, Kaplan-Meier survival curves of glioma-bearing mice (log-rank test, considered significant for $p<0.05$). G, Angiogenic gene expression heatmaps obtained by unsupervised comparison of genes differentially expressed in the four mouse glioma cell lines. The heatmaps indicate high to low expression levels as red to blue color coding. Up- or downregulated gene clusters in SMA-497 and GL-261 cells are encircled in red or blue.

Fig. 3 Differential effects of LY2157299 on the growth of murine gliomas. Mice intracranially implanted with SMA-497, SMA-540, SMA-560 or GL-261 cells were treated daily with LY2157299 at 150 mg/kg or control solvent from day 7 on. Brain sections (early-stage) were analysed. A, Tumor volumes. B, pSMAD2 and CD31+ capillaries (C). Data are

expressed as mean and SEM (*p<0.05, ****p<0.0001, unpaired student t-test, LY2157299 versus solvent). D, Kaplan-Meier survival curves of glioma-bearing mice (log-rank test was considered significant for p<0.05). E,F, Gene expression heatmaps were obtained by unsupervised comparison of genes differentially expressed in the four mouse glioma cell lines for the TGF-β signaling (E) and immune response (F) pathways. The heatmaps indicate high to low expression levels as red to blue color coding. Up- or downregulated gene clusters in SMA-497 and GL-261 cells are encircled in red or blue.

Fig. 4 Effect of combined B20 and LY2157299 treatment in SMA-497 and GL-261 syngeneic models in vivo. Syngeneic mice were intracranially implanted with SMA-497 or GL-261 cells and treated twice weekly with 5 mg/kg B20 or daily with 150 mg/kg LY2157299 or corresponding solvents or both from day 7 on. Brain sections from SMA-497 (early-stage) and GL-261 (early- and end-stage) were studied. Tumor volumes (A) and CD31+ capillaries (B). C, pSMAD2 . D, CA IX+ areas (*p<0.05, **p<0.01, ***p<0.001, one-way ANOVA followed by Tukey's post hoc test confidence interval 95%, treated versus solvent, +++p<0.001, B20+LY2157299 versus B20, ##p<0.01, B20+LY2157299 versus LY2157299). E, Kaplan-Meier survival curves (Gehan-Breslow-Wilcoxon test, considered significant for p<0.05). F, Gene cluster analysis. Functional interactions between TGF-β1/2 and genes upregulated in angiogenic profiles in SMA-497 (left) and GL-261 (right) were analyzed in Affymetrix micro-array based gene expression profiling by STRING analysis. Interactions with high confidence score of 0.700 were integrated to the interactome. Clusters were determined by MCL algorithm and presented with different node colors. Inter-cluster edges are represented by dashed-lines.

Fig. 5 Modulation of tumor immune cell infiltration in combined B20- and LY2157299-treated syngeneic models in vivo. Brain sections from SMA-497 (early-stage) and GL-261 (early- and end-stage) were examined. A, CD45+ leukocytes. B, CD4+ T helper cells. C,

CD8+ cytotoxic T cells. D, CD11b+ monocytes/microglia. Data are expressed as mean and SEM (*p<0.05 and **p<0.01, ***p<0.001 one-way ANOVA followed by Tukey's post hoc test confidence interval 95%, treatment versus solvent, #p<0.05, B20+LY2157299 versus LY2157299, +p<0.05 B20+LY2157299 versus B20).

Fig. 6 Modulation of pSMAD2 levels and tumor immune cell infiltration in B20 and LY2157299 co-treated GL-261 syngeneic model in vivo. Brain sections (end-stage) were examined. Staining of tumor sections was assessed with DAPI (A, blue), pSMAD2 (B, green) and CD45 (C, red). Merged images are shown in (D). CD45+/pSMAD2+ leukocytes are marked by arrow heads. Size bars correspond to 50 μm.

Figure 1

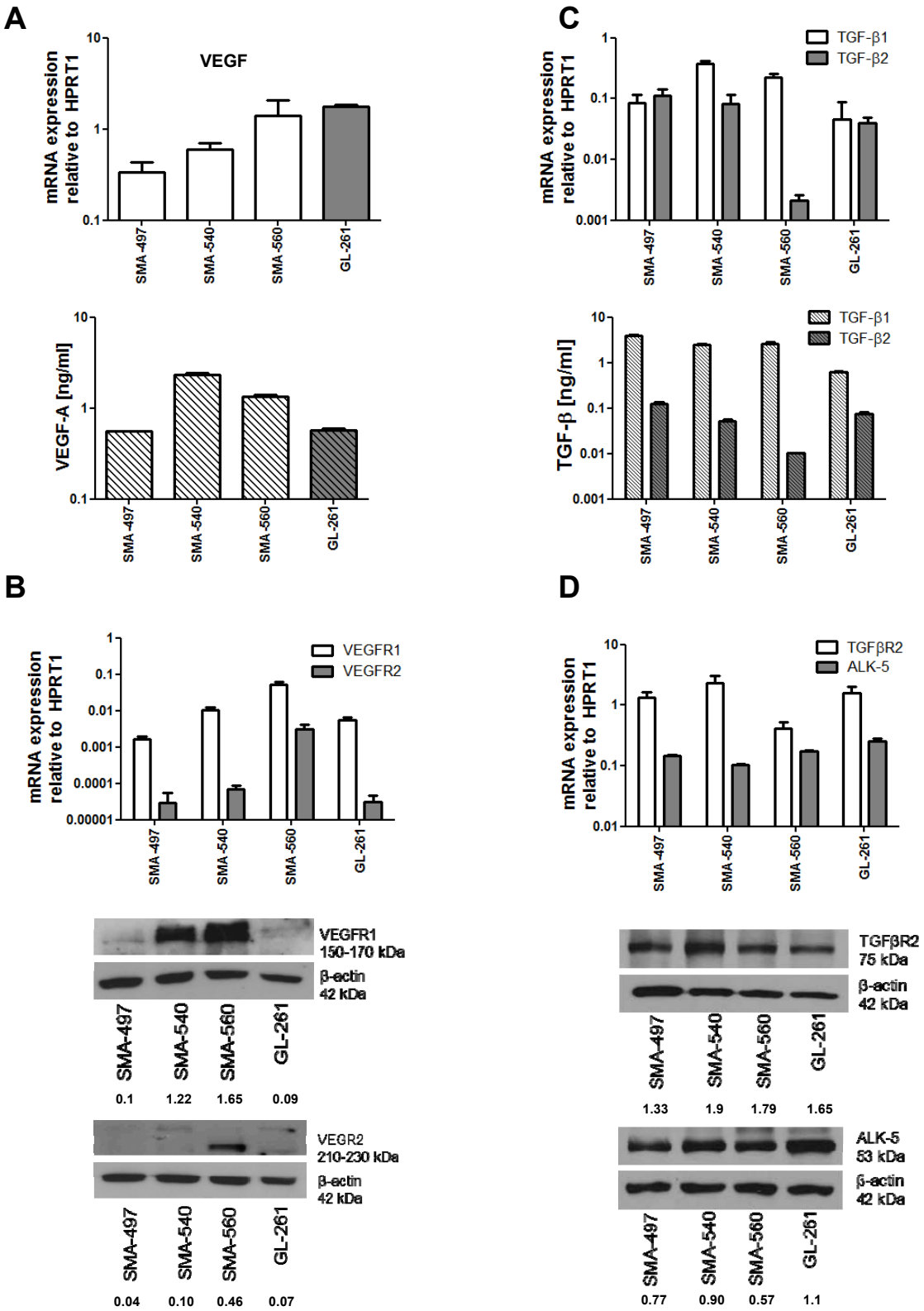
A
VEGF
mRNA expression relative to HPRT1
10
1
0.1
SMA-497
SMA-540
SMA-560
GL-261
VEGF-A [ng/ml]
10
1
0.1
SMA-497
SMA-540
SMA-560
GL-261
C
TGF-β1
TGF-β2
mRNA expression relative to HPRT1
1
0.1
0.01
0.001
SMA-497
SMA-540
SMA-560
GL-261
TGF-β1
TGF-β2
TGF-β [ng/ml]
10
1
0.1
0.01
0.001
SMA-497
SMA-540
SMA-560
GL-261
B
VEGFR1
VEGFR2
mRNA expression relative to HPRT1
1
0.1
0.01
0.001
0.0001
0.00001
SMA-497
SMA-540
SMA-560
GL-261
VEGFR1
150-170 kDa
β-actin
42 kDa
SMA-497
SMA-540
SMA-560
GL-261
0.1
1.22
1.65
0.09
VEGR2
210-230 kDa
β-actin
42 kDa
SMA-497
SMA-540
SMA-560
GL-261
0.04
0.10
0.46
0.07
D
TGFβR2
ALK-5
mRNA expression relative to HPRT1
10
1
0.1
0.01
SMA-497
SMA-540
SMA-560
GL-261
TGFβR2
75 kDa
β-actin
42 kDa
SMA-497
SMA-540
SMA-560
GL-261
1.33
1.9
1.79
1.65
ALK-5
53 kDa
β-actin
42 kDa
SMA-497
SMA-540
SMA-560
GL-261
0.77
0.90
0.57
1.1

Figure 2

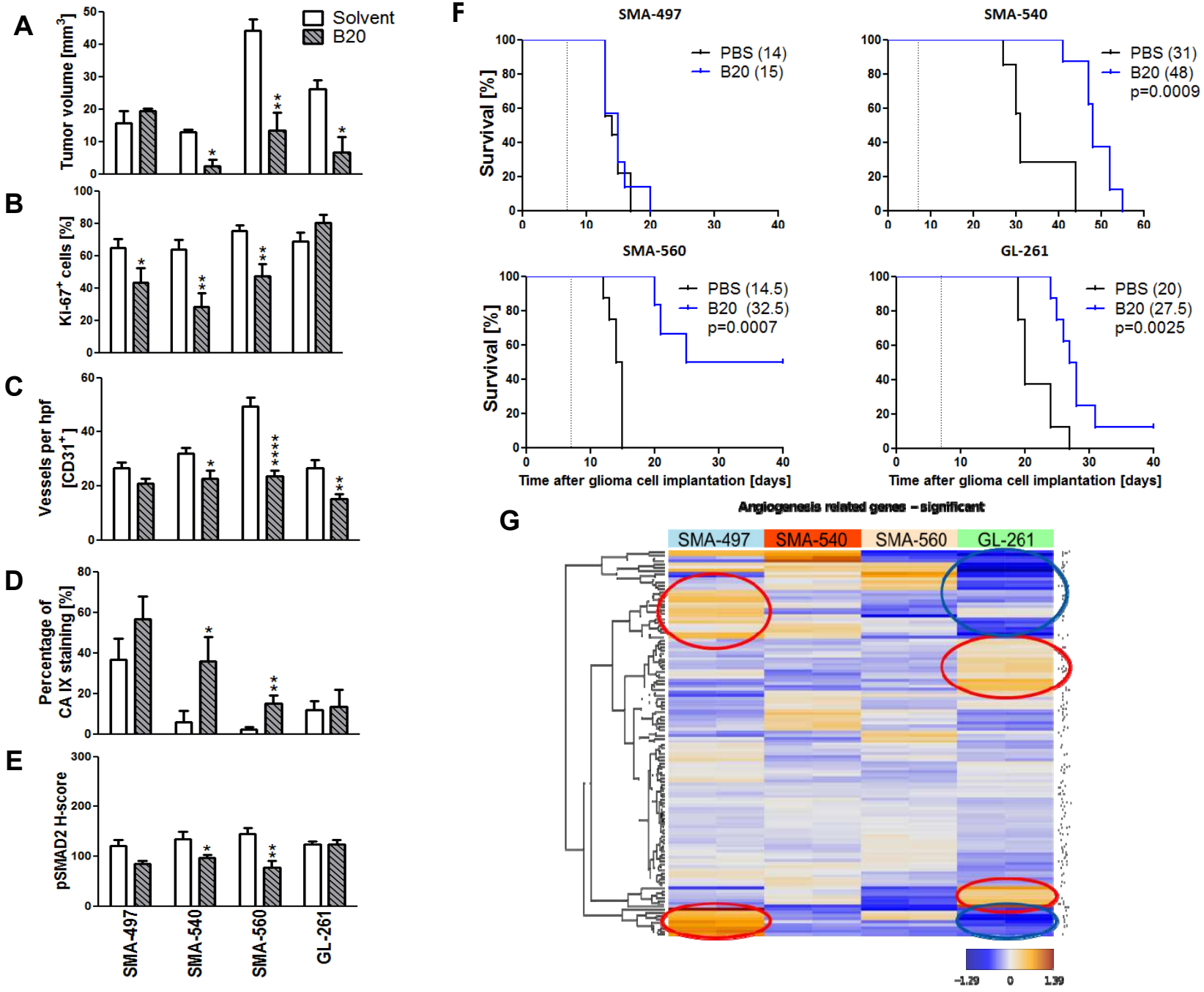
A
Solvent
B20
Tumor volume [mm³]
B
Ki-67⁺ cells [%]
C
Vessels per hpf [CD31⁺]
D
Percentage of CA IX staining [%]
E
pSMAD2 H-score
SMA-497
SMA-540
SMA-560
GL-261
F
SMA-497
PBS (14)
B20 (15)
SMA-540
PBS (31)
B20 (48)
p=0.0009
SMA-560
PBS (14.5)
B20 (32.5)
p=0.0007
GL-261
PBS (20)
B20 (27.5)
p=0.0025
Survival [%]
Time after glioma cell implantation [days]
G
Angiogenesis related genes – significant
SMA-497
SMA-540
SMA-560
GL-261
-1.29
0
1.39

Figure 3

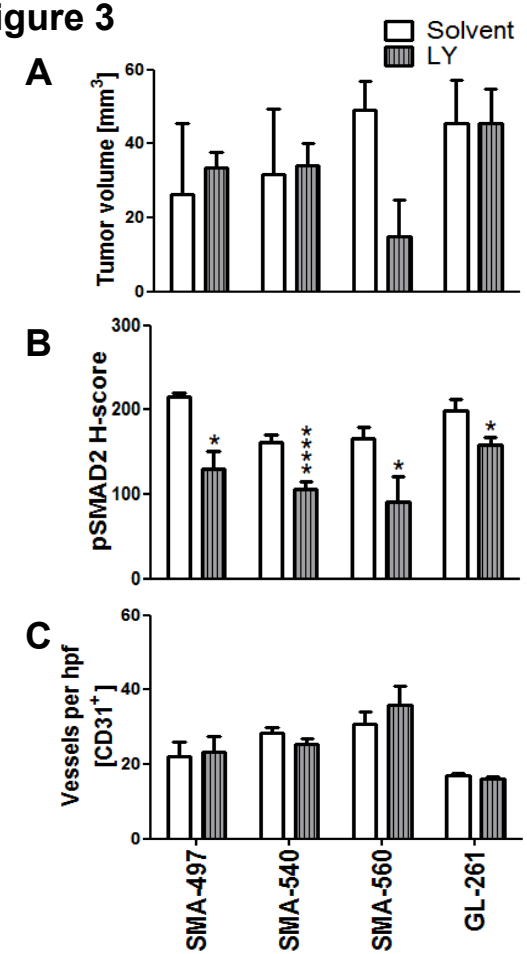
A
Solvent
LY
Tumor volume [mm3]
B
pSMAD2 H-score
C
Vessels per hpf [CD31+]
SMA-497
SMA-540
SMA-560
GL-261

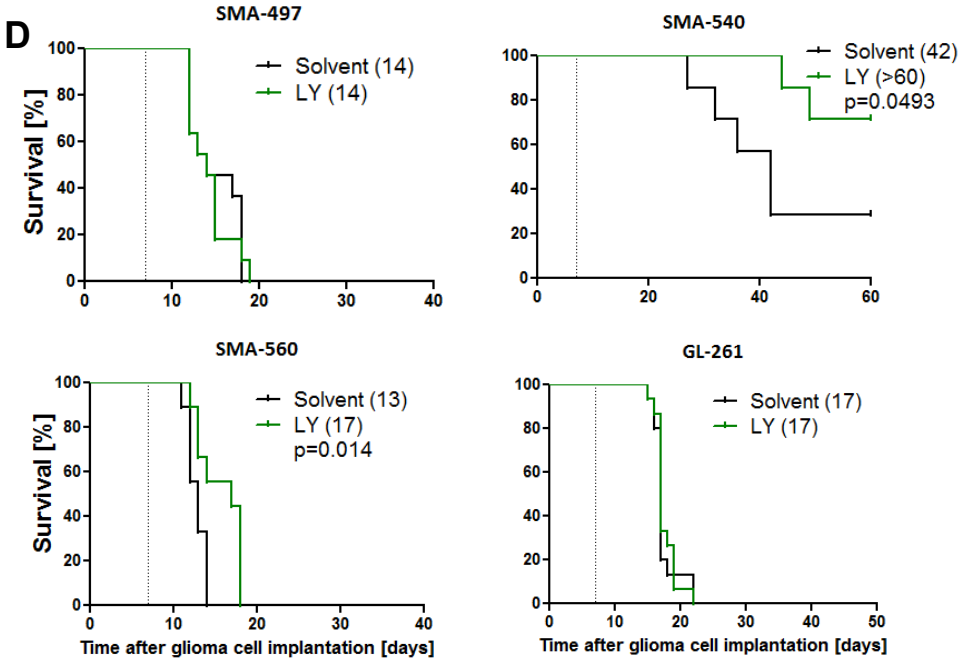
D
SMA-497
Solvent (14)
LY (14)
SMA-540
Solvent (42)
LY (>60)
p=0.0493
SMA-560
Solvent (13)
LY (17)
p=0.014
GL-261
Solvent (17)
LY (17)
Survival [%]
Time after glioma cell implantation [days]

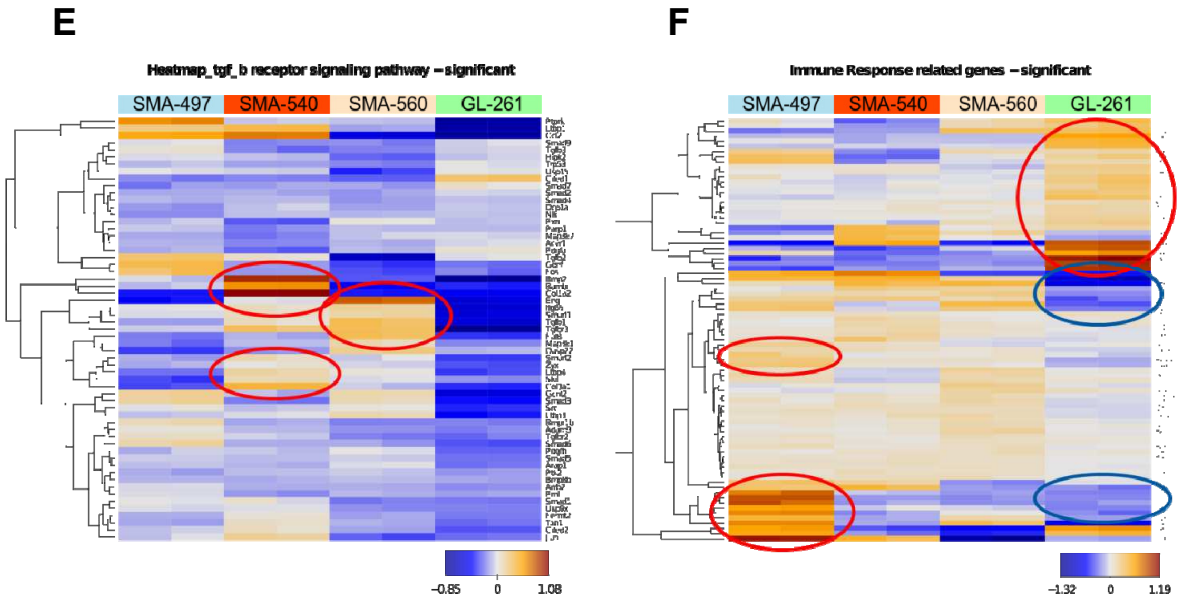
E
Heatmap_tgf_b receptor signaling pathway – significant
SMA-497
SMA-540
SMA-560
GL-261
F
Immune Response related genes – significant

Figure 4

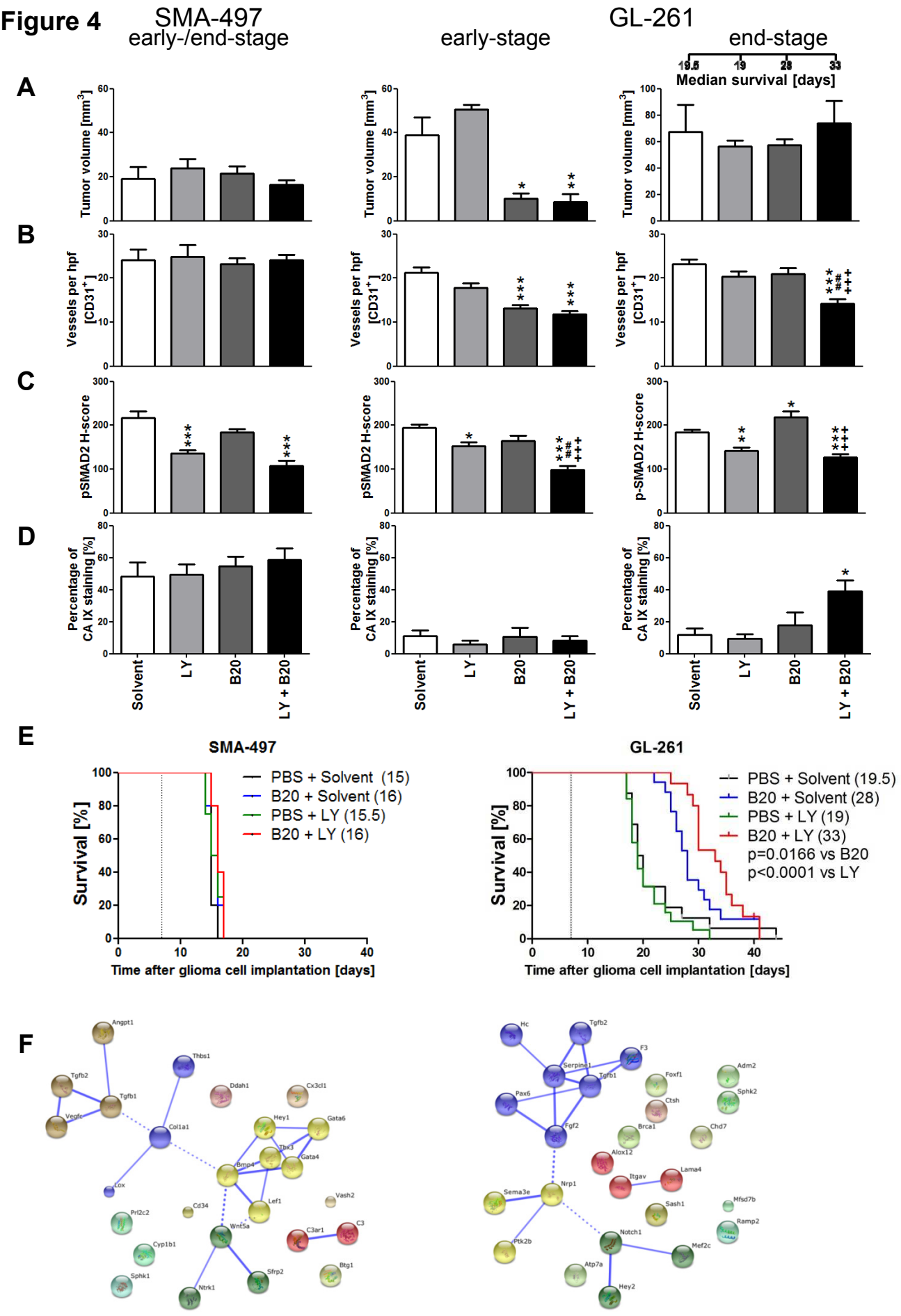
SMA-497
early-/end-stage
GL-261
early-stage
end-stage
Median survival [days]
19.5
19
28
33
A
B
C
D
Tumor volume [mm3]
Vessels per hpf [CD31+]
pSMAD2 H-score
p-SMAD2 H-score
Percentage of CA IX staining [%]
Solvent
LY
B20
LY + B20
E
SMA-497
GL-261
Survival [%]
Time after glioma cell implantation [days]
PBS + Solvent (15)
B20 + Solvent (16)
PBS + LY (15.5)
B20 + LY (16)
PBS + Solvent (19.5)
B20 + Solvent (28)
PBS + LY (19)
B20 + LY (33)
p=0.0166 vs B20
p<0.0001 vs LY
F

Figure 5

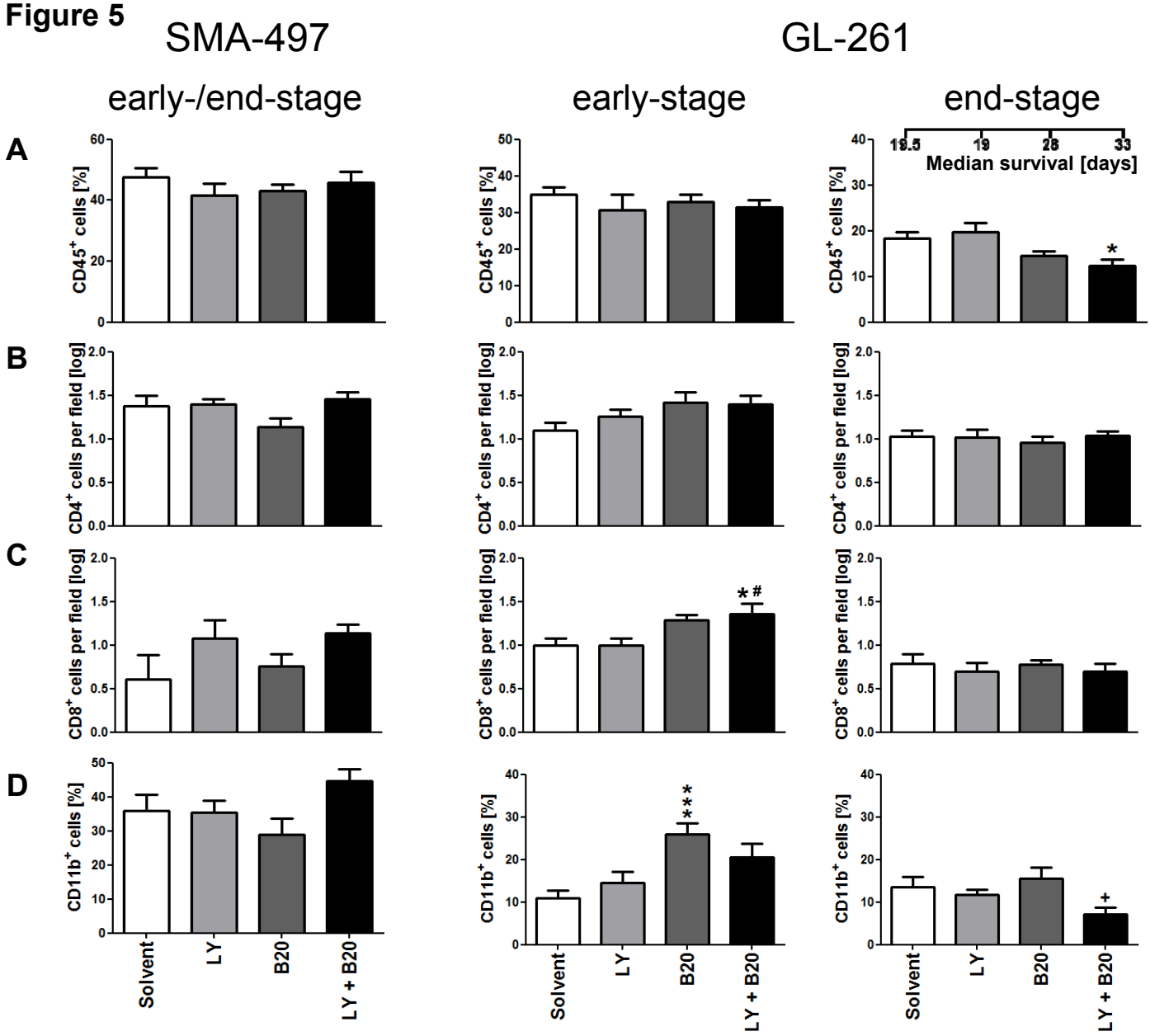
SMA-497
GL-261
early-/end-stage
early-stage
end-stage
A
B
C
D
CD45+ cells [%]
CD4+ cells per field [log]
CD8+ cells per field [log]
CD11b+ cells [%]
Median survival [days]
19.5
19
28
33
*
*#
***
+
Solvent
LY
B20
LY + B20

Figure 6

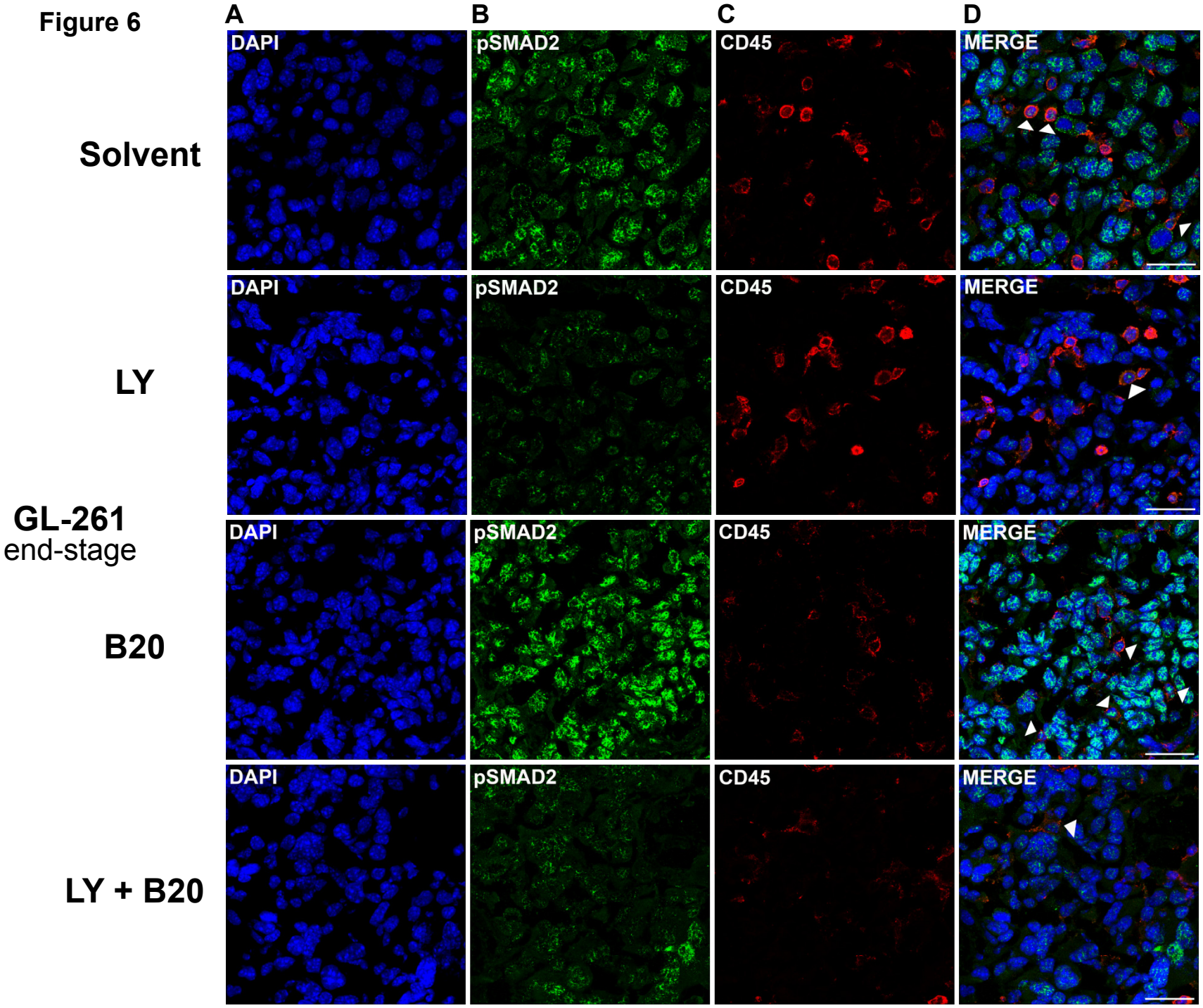
A
B
C
D
DAPI
pSMAD2
CD45
MERGE
Solvent
LY
GL-261
end-stage
B20
LY + B20

Supplementary Figure 1

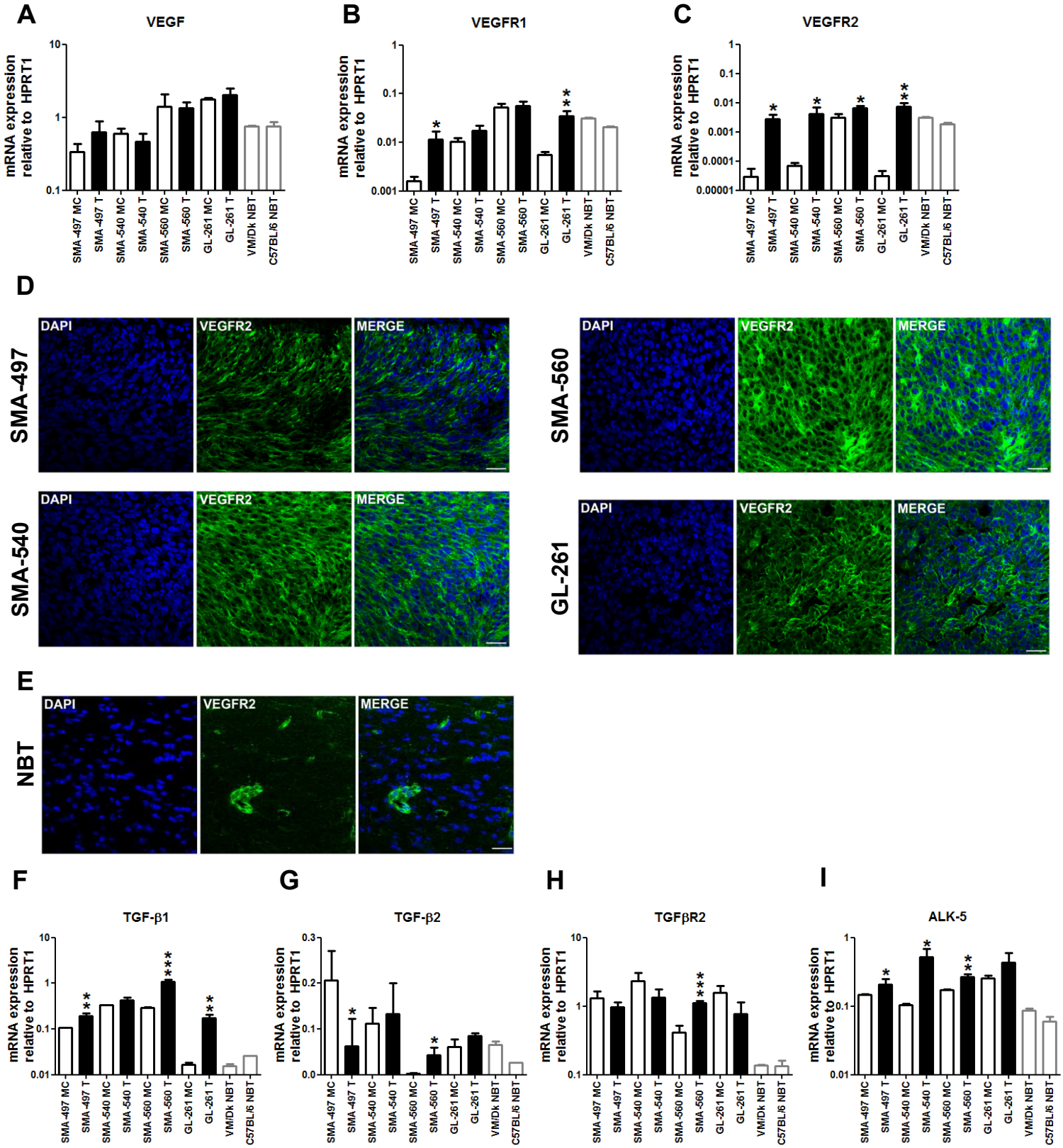

Supplementary Figure 2

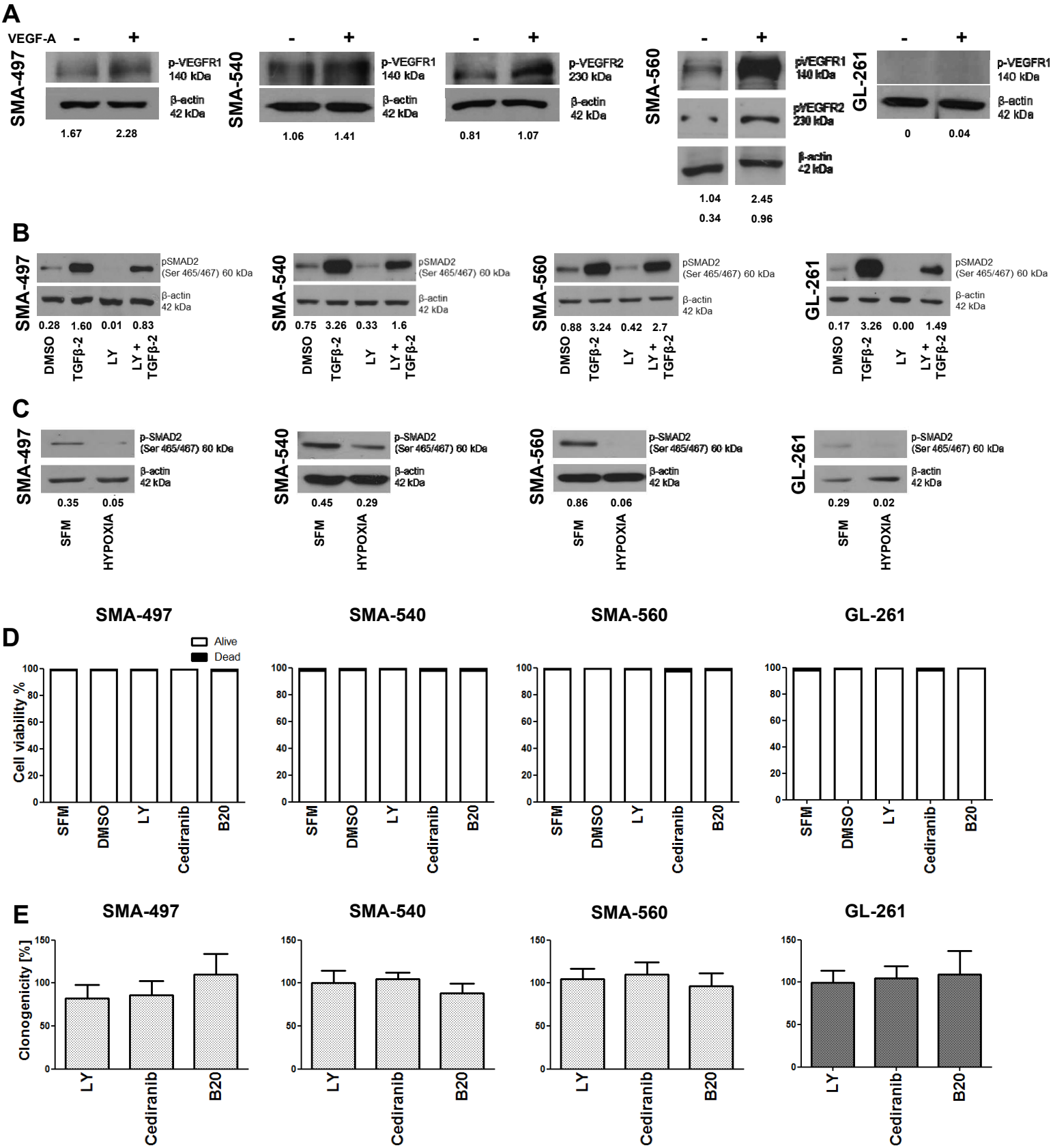

Supplementary Figure 3

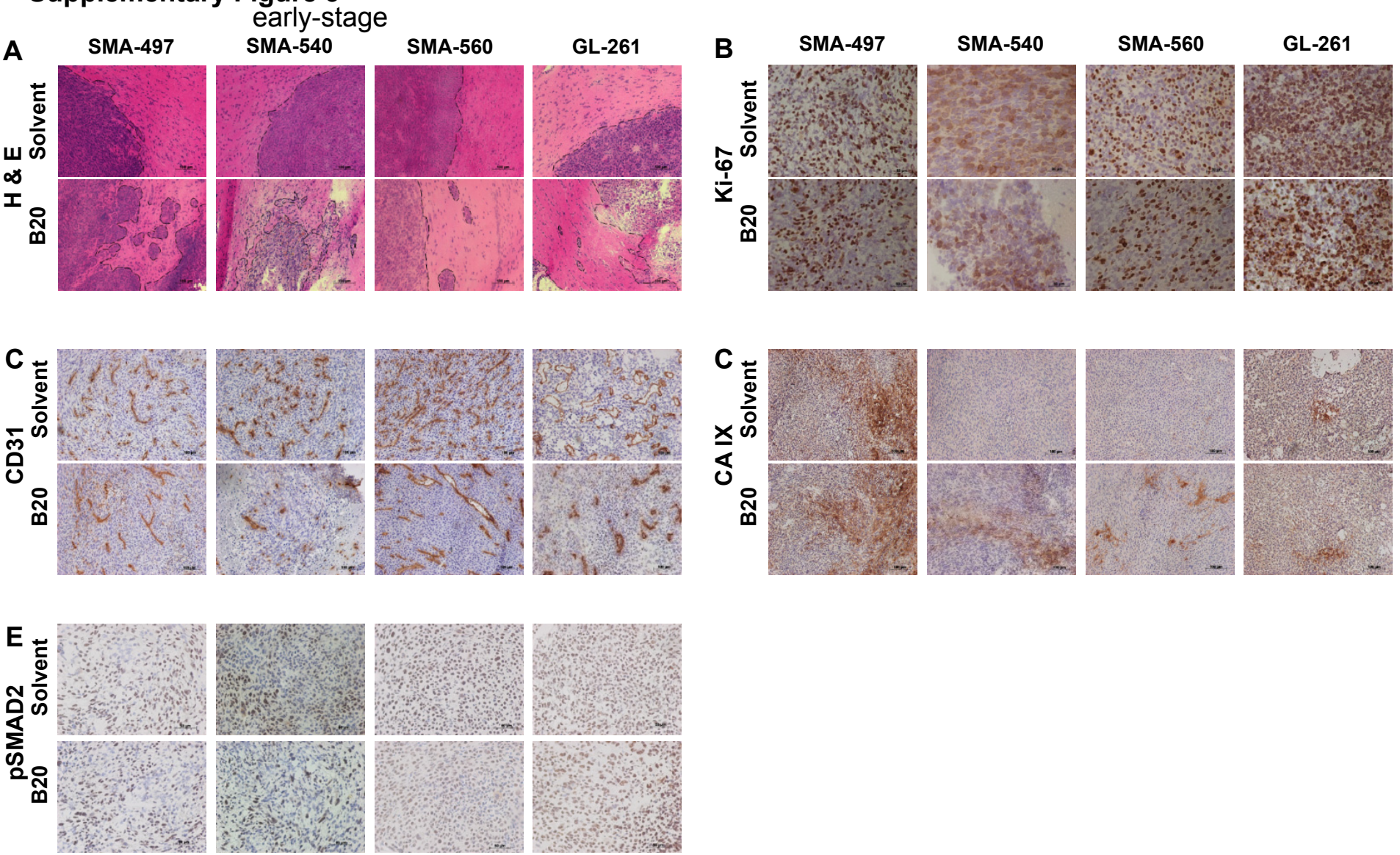

Supplementary Figure 3

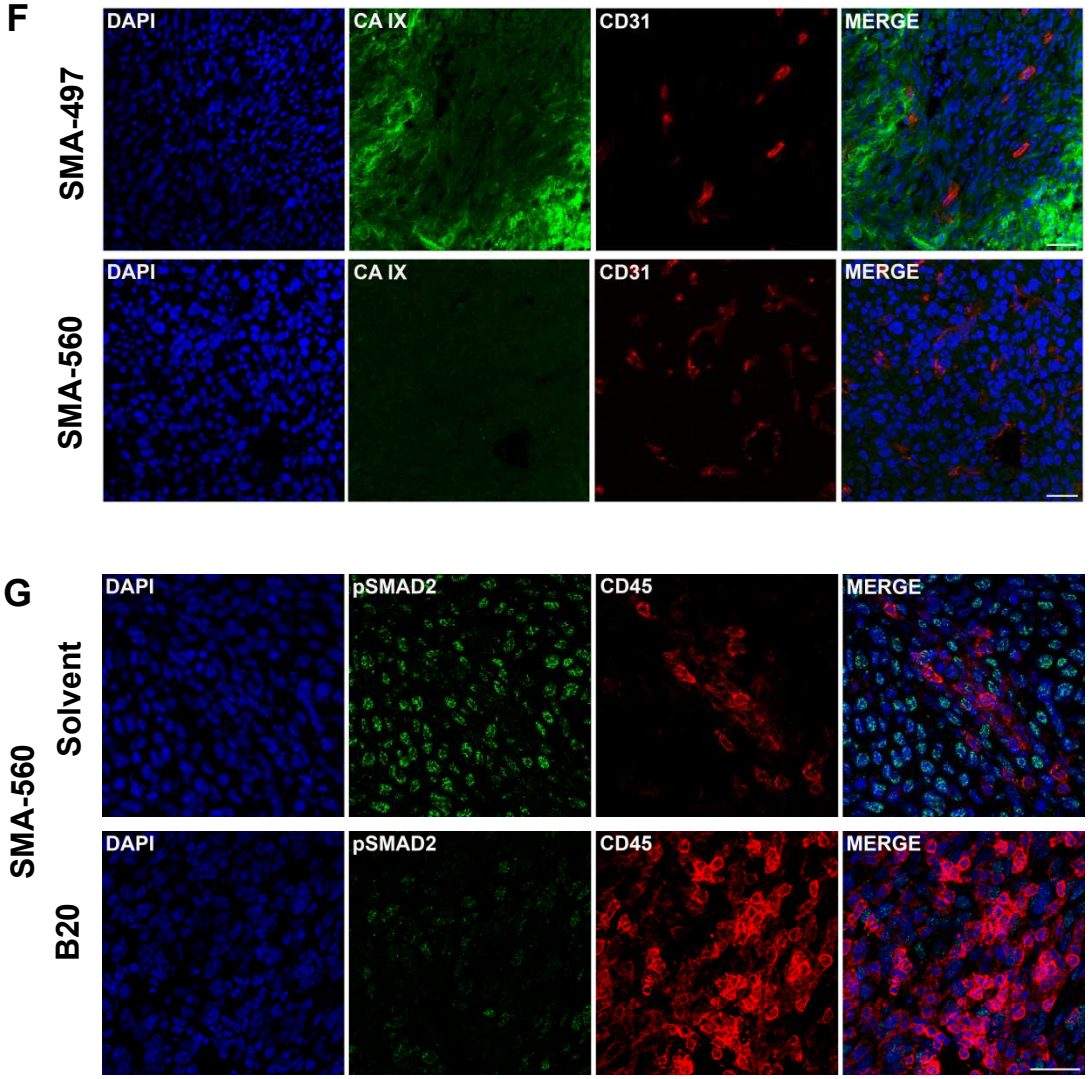

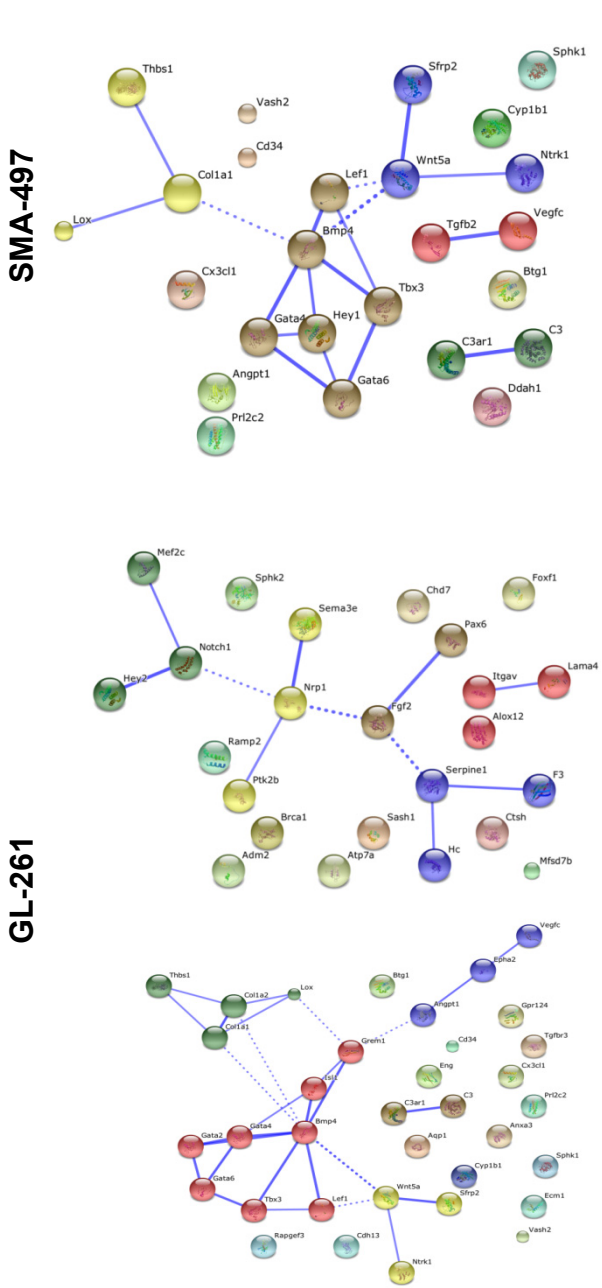

Supplementary Figure 4

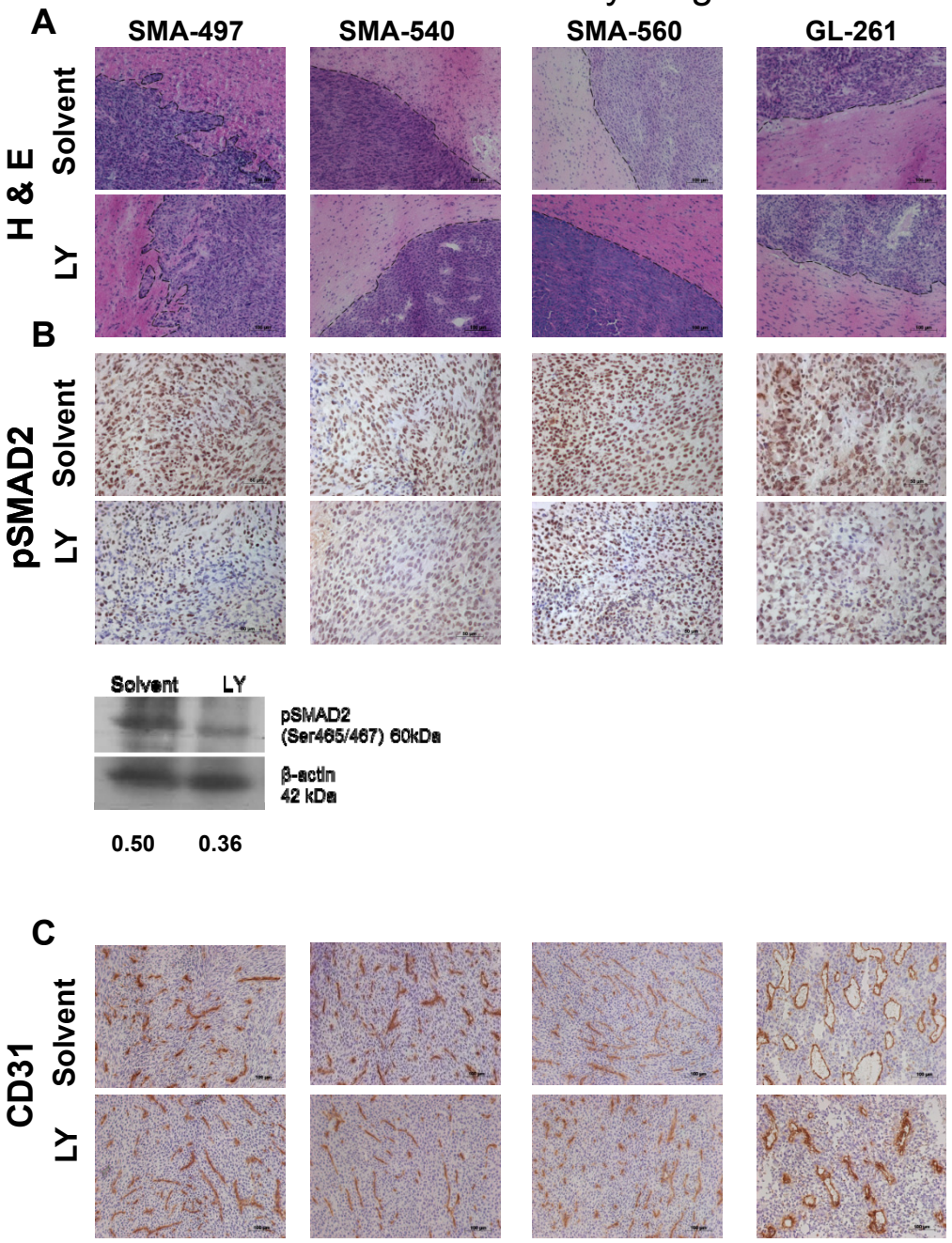

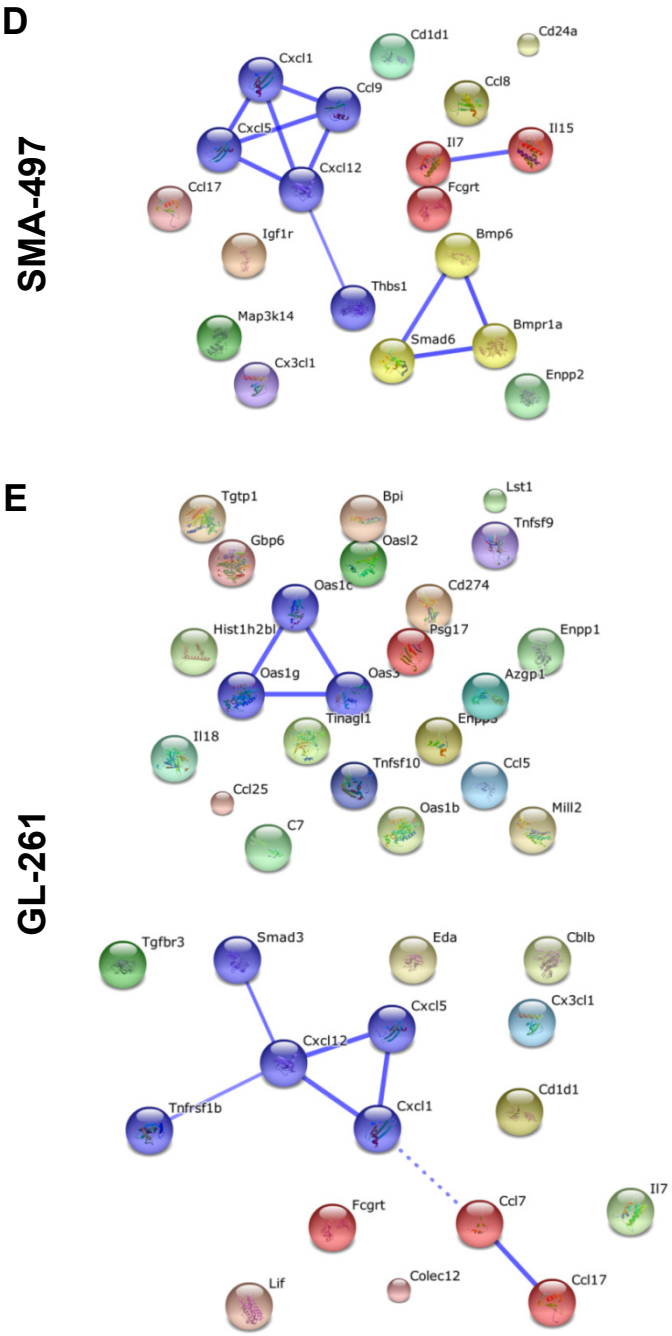

Supplementary Figure 5

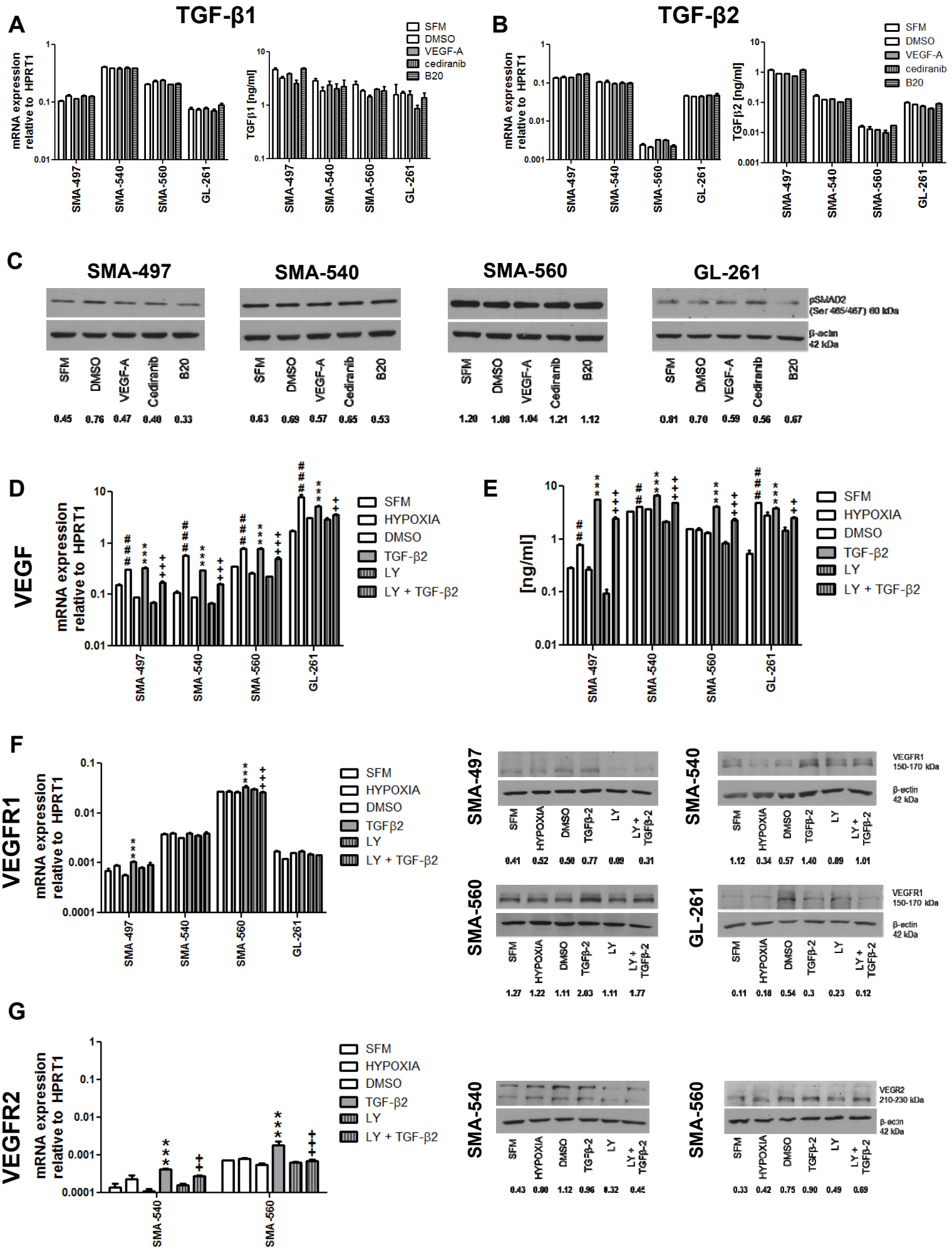

Supplementary Figure 6

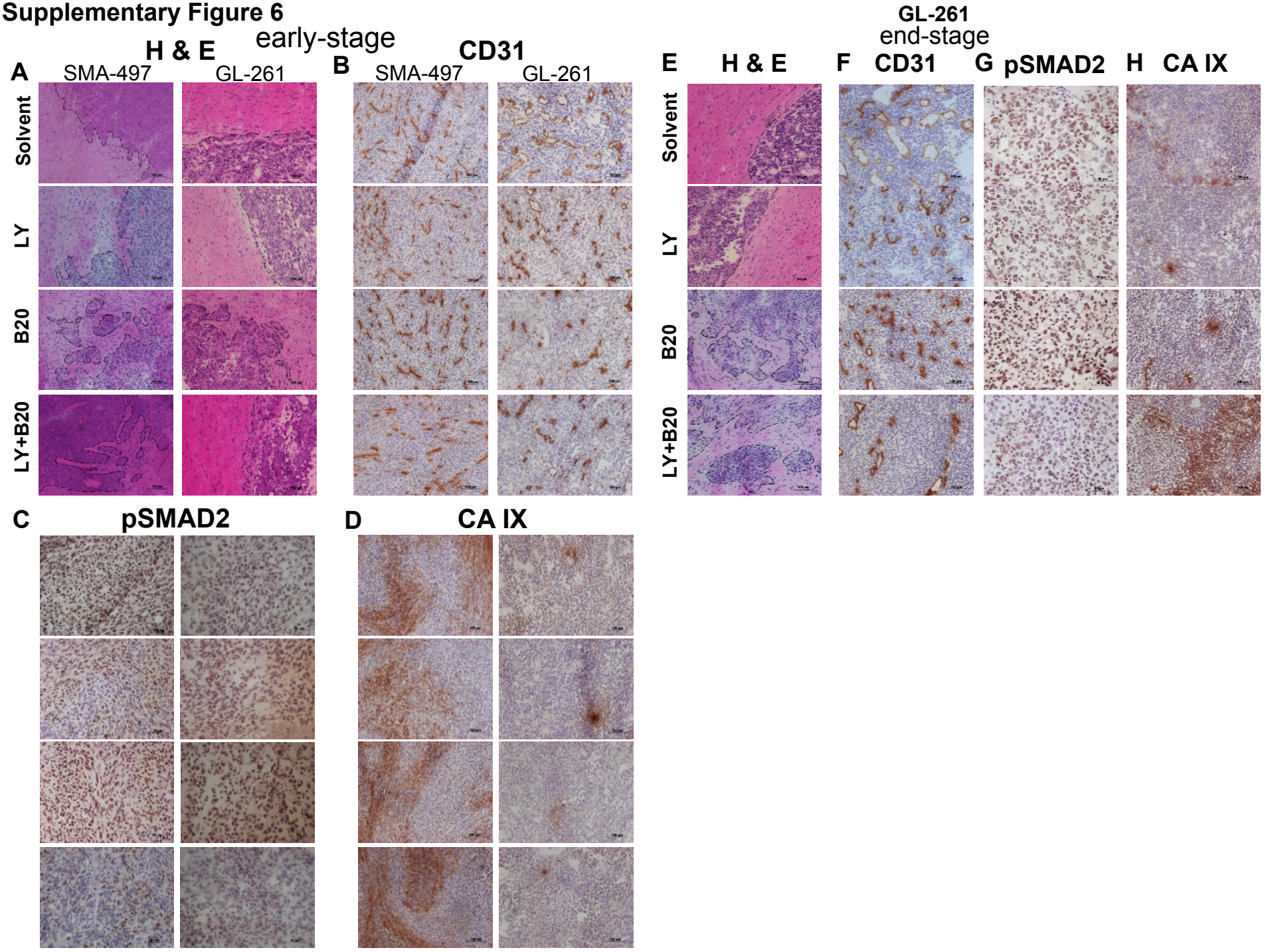

Supplementary Figure 6

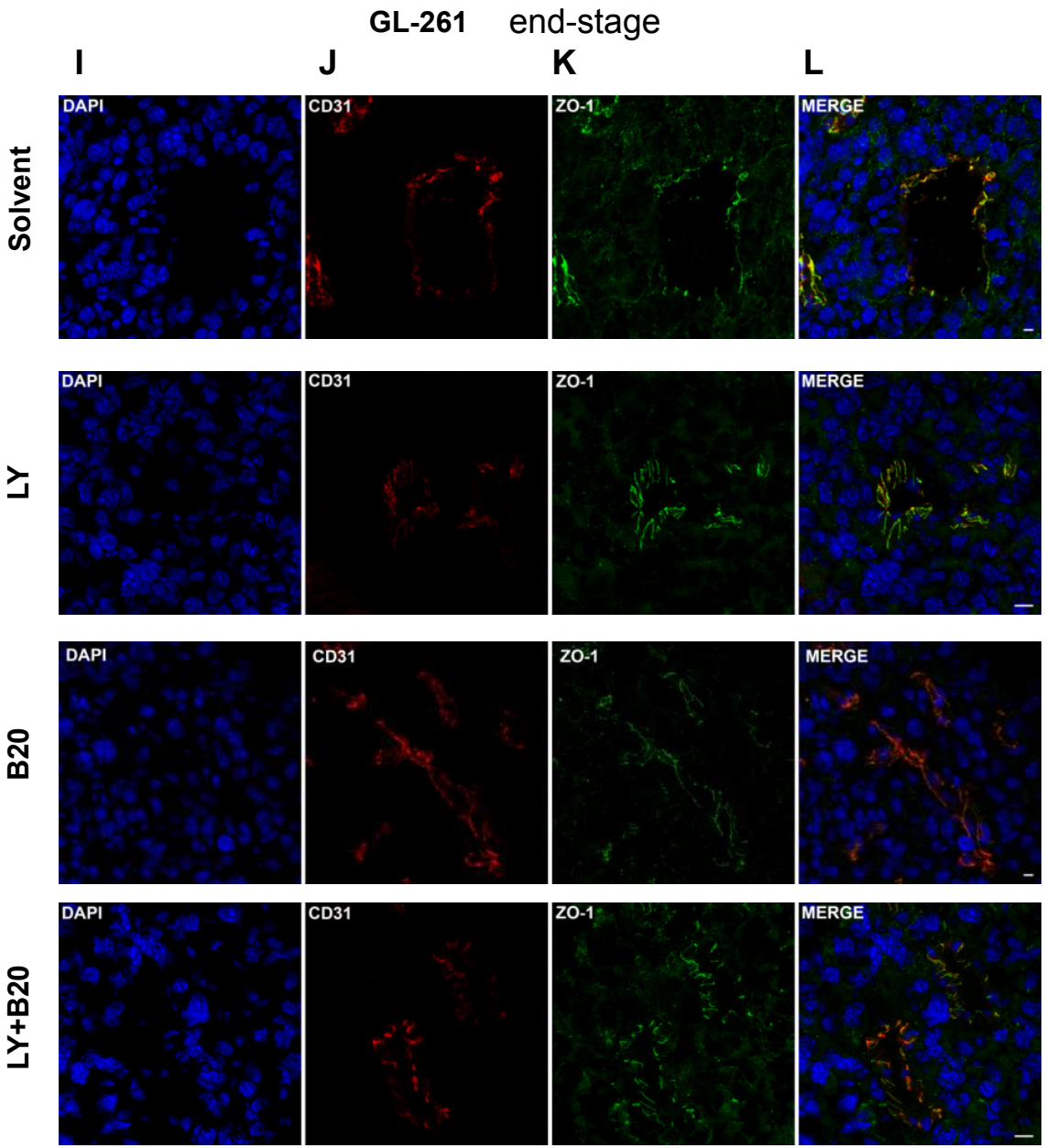

Supplementary Figure 7

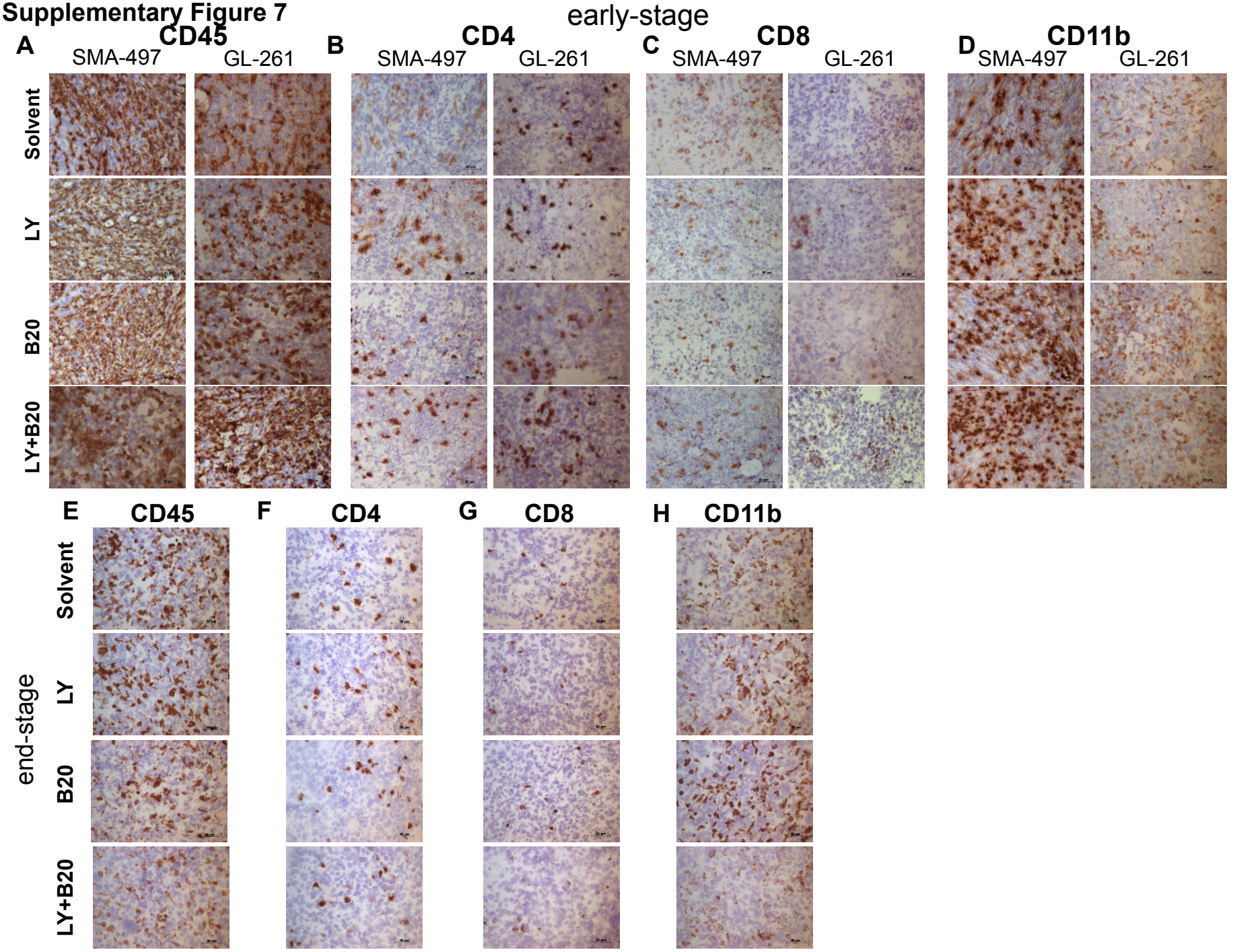

Supplementary Figure 8

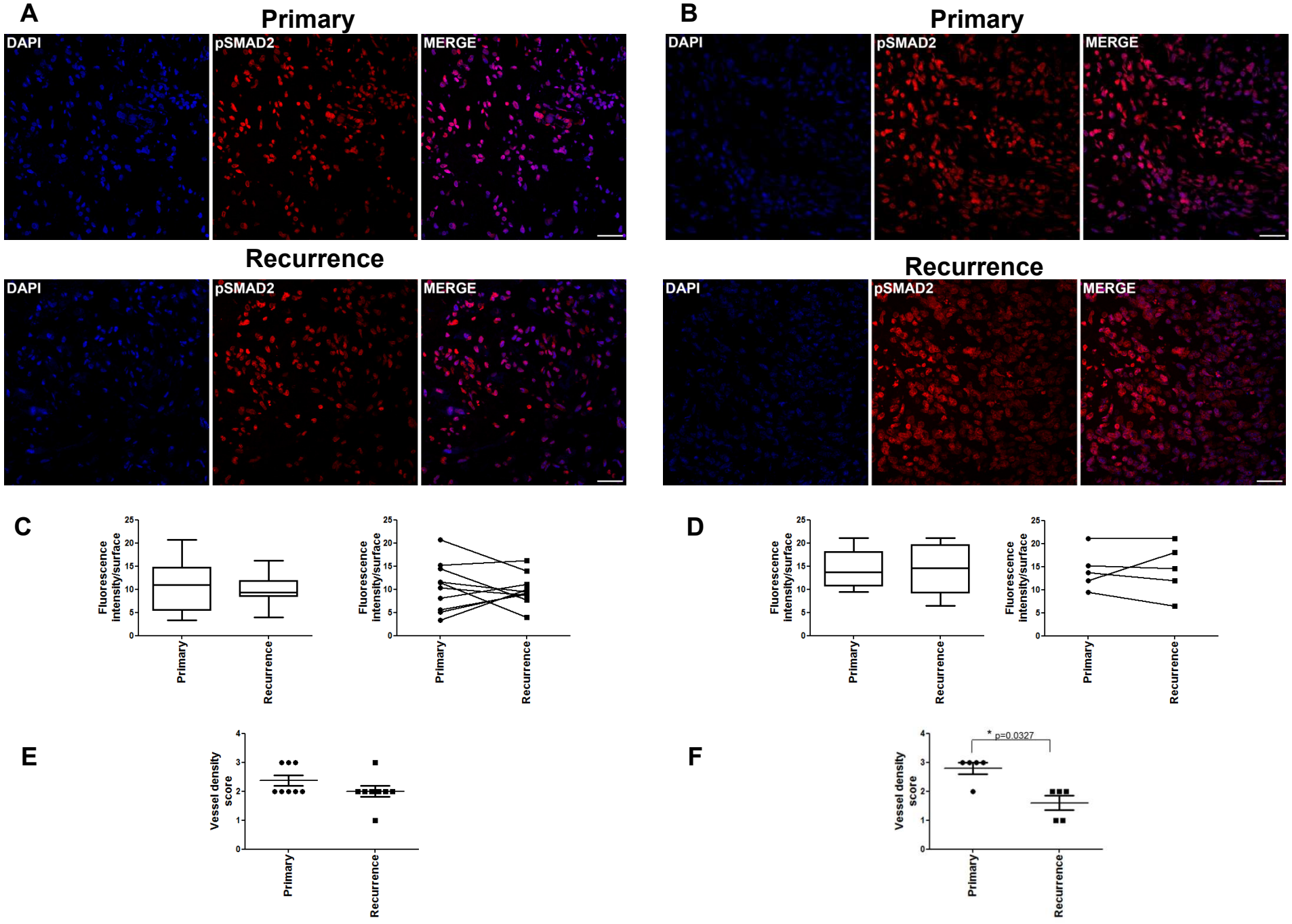

Supplementary Table 1. Sensitivity of mouse glioma models to VEGF antibody B20 or the TGF-βR1 (ALK-5) antagonist LY2157299 alone or their combination *in vivo.*

	Cell line			
	SMA-497	**SMA-540**	**SMA-560**	**GL-261**
	Median survival (range) [days]			
Treatment				
Control	14 (13–17)	31 (27–44)	14.5 (12–14)	20 (19-24)
B20	15 (13–20)	48 (41–55)	32.5 (20->40*)	27.5 (24->40*)
	ns	p=0.0009	p=0.0007	p=0.0025
Control	14 (12–18)	42 (27->60*)	13 (11–14)	17 (15 – 22)
LY2157299	14 (12–19)	>60 (44->60*)	17 (12 – 18)	17 (15–22)
	ns	ns	p=0.014	ns
Control	15 (14–16)			19.5 (17–44)
B20	15 (14–17)			28 (22–41)
LY2157299	15.5 (14–17)			19 (17–32)
B20+LY2157299	16 (15–17)			33 (25–41)
	ns			p=0.0166 (cotreatment vs B20) p<0.0001 (cotreatment vs LY)

* censored because experiment was terminated at day 40 or day 60

Supplementary Table 2. Gene sets of angiogenic profiles as defined by Gene Ontology classification schemes.

Angiogenesis related genes (all genes analysed)						
Ctsh	*Col1a1*	*Wnt5a*	*Gata6*	*Sfrp2*	*Kdr*	*Hmox1*
Cdc42	*Dlx3*	*Gdf2*	*Fgf1*	*Gja5*	*Tgfbr3*	*Cx3cl1*
Pdcl3	*Ramp2*	*Loxl2*	*Lox*	*F3*	*Ccl24*	*Cdh13*
Col3a1	*Map3k3*	*Bmp4*	*Ccbe1*	*Lef1*	*Serpine1*	*Foxf1*
Cxcr2	*Sphk1*	*Cma1*	*Tcf7l2*	*Ddah1*	*Cdx2*	*Foxc2*
Chil1	*Uts2r*	*Gata4*	*Nrarp*	*Hey1*	*Flt1*	*Nrp1*
Tnfsf4	*Prop1*	*Ptk2b*	*Egfl7*	*Agtr1b*	*Col1a2*	*Angpt2*
Cd34	*Alox12*	*Cysltr2*	*Col5a1*	*Rapgef2*	*Aqp1*	*Gatad2a*
Tgfb2	*Brca1*	*C6*	*Rapgef1*	*Ntrk1*	*Gata2*	*Agt*
Vash2	*Prkca*	*Mtdh*	*Eng*	*Ecm1*	*Tnfrsf1a*	*Ets1*
Mfsd7b	*Jmjd6*	*Adm2*	*Itgav*	*Chd7*	*Hipk2*	*Stra6*
Cited2	*Hif1a*	*Acvrl1*	*Pax6*	*Tek*	*Epha1*	*Aldh1a2*
Lama4	*Psen1*	*Otulin*	*Thbs1*	*Angptl3*	*C3ar1*	*Ccr3*
Nodal	*Rhob*	*Angpt1*	*Angpt4*	*Ppap2b*	*Prkd2*	*Camp*
Itgb2	*Prkd1*	*Ptk2*	*Plcg1*	*Epha2*	*Psg22*	*Tgfbr2*
Tbxa2r	*Pgf*	*Pdgfb*	*Notch1*	*Uts2*	*Rras*	*Cx3cr1*
Btg1	*Agtr1a*	*Rapgef3*	*Hc*	*Shb*	*Fzd4*	*Cdx4*
E2f7	*Foxc1*	*Crkl*	*Grem1*	*Tie1*	*Adm*	*Atp7a*
Sash1	*Erap1*	*Tbx1*	*Il1a*	*Gja4*	*Parva*	*Cxcr3*
Hey2	*Mef2c*	*Pkd1*	*Il1b*	*Sema3e*	*Prkcb*	*Cysltr1*
Nr2e1	*Esm1*	*Vegfa*	*Foxs1*	*Hgf*	*Dhcr7*	*Chm*
Ccm2	*Prl2c2*	*Lrg1*	*Ptgis*	*Nos3*	*Sphk2*	*Esx1*
Flt4	*Pdcd6*	*C3*	*Sox18*	*Add1*	*E2f8*	
Pik3r6	*Aggf1*	*Cyp1b1*	*Fgf2*	*Anxa3*	*Gpr124*	
Ccl11	*Isl1*	*Mib1*	*Foxo1*	*Tbx3*	*Vegfc*	

Supplementary Table 3. Differentially regulated genes of angiogenic profiles of SMA-497 and GL-261 mouse glioma cell lines, as defined by Gene Ontology classification schemes.

Angiogenesis-related genes up-regulated in SMA-497	**Angiogenesis-related genes up-regulated in GL-261**	**Angiogenesis related genes down-regulated in GL-261**
C3; Col1a1; Wnt5a; Lef1; Tbx3; Btg1; Vash2; Gata4; Tgfb2; Ddah1 Hey1; Thbs1; Gata6 Prl2c2; Lox; Sphk1 CD34; Cyp1b1; Ntrk1 Sfrp2; Angpt1; Vegfc; Cx3cl1; Bmp4; C3ar1	*Chd7; Serpine1; Sema3e; Notch1; Hc; Itgav; Brca1; Foxf1; Ramp2; Hey2; Alox12; Ptk2b; Adm2; Nrp1; Mfsd7b; Sphk2; Otulin; Ctsh; F3; Lama4; Mef2c; Pax6; Sash1; Fgf2; Atp7a*	*Col1a1; Wnt5a; Lef1; Tbx3; Btg1; Vash2 Gata4; Thbs1; Gata6 Prl2c2; Lox; Sphk1 C3; Ecm1; Rapgef3 Gata2; Isl1; Aqp1;Eng Anxa3; Tgfbr3; Epha2 Col1a2; Grem1;Cdh13 Gpr124; CD34; Cyp1b1; Ntrk1; Sfrp2; Angpt1; Vegfc; Cx3cl1; Bmp4; C3ar1*

Supplementary Table 4. Gene sets of TGF-β receptor signaling pathways as defined by Gene Ontology classification schemes.

TGF-β receptor signaling pathway related genes (all genes analysed)					
Col3a1	*Wfikkn2*	*Tab1*	*Eng*	*Bmp8a*	*Smad1*
Mstn	*Smurf2*	*Acvrl1*	*Bmp2*	*Pxn*	*Pml*
Parp1	*Smurf2*	*Amhr2*	*Src*	*Tgfbr3*	*Smad3*
Tgfb2	*Fut8*	*Ptk2*	*Acvr1*	*Pdgfa*	*Smad6*
Cited2	*Fos*	*Foxh1*	*Fshb*	*Smurf1*	*Tgfbr2*
Ptprk	*Tgfb3*	*Pdgfb*	*Dusp15*	*Col1a2*	*Usp9x*
Nodal	*Dusp22*	*Itgb5*	*Skil*	*Zyx*	*Cited1*
Usp15	*Gcnt2*	*Ltbp1*	*Smad9*	*Hipk2*	
Trp53	*Smad5*	*Bambi*	*Bmpr1b*	*Tgfb1*	
Arrb2	*Map3k1*	*Smad7*	*Map3k7*	*Arap1*	
Ccl2	*Dcp1a*	*Smad2*	*Tgfbr1*	*Ltbp4*	
Nlk	*Fermt2*	*Smad4*	*Bmp8b*	*Hpgd*	
Wfikkn2	*Gdnf*	*Ltbp3*	*Jun*	*Adam9*	

Supplementary Table 5. Differentially regulated genes of TGF-β signaling pathways of SMA-540 and SMA-560 mouse glioma cell lines, as defined by Gene Ontology classification schemes.

TGF-β-related genes up-regulated in SMA-540	TGF-β-related genes up-regulated in SMA-560
Tgfbr3; Tgfb1; Smurf1; Itgb5; Eng; Col1a2; Bambi; Bmp2; Col3a1; Skil; Ltbp4; Zyx: Smurf2	*Dusp22; Map3k1 Fut8; Tgfbr3; Tgfb1 Smurf1; Itgb5; Eng*

Supplementary Table 6. Gene sets of immunogenic profiles as defined by Gene Ontology classification schemes.

Immune response related genes (all genes analysed)					
Ilf2	*Ccl1*	*H2-M11*	*Thbs1*	*Oas3*	*Myd88*
Oprk1	*Ccl5*	*H2-M10.5*	*Procr*	*Oas1e*	*Ccr1*
Zap70	*Ccl9*	*H2-M10.6*	*Bpi*	*Oas1c*	*Ccr1l1*
Cd28	*Ccl6*	*Tnfsf9*	*Il1a*	*Oas1g*	*Ccr5*
Ctla4	*Ccr7*	*Vav1*	*Il1b*	*Ccl26*	*Ccl28*
Ccl20	*Ccr10*	*H2-K1*	*Tnfsf10*	*Ccl24*	*Eda*
Fcamr	*Map3k14*	*Lst1*	*Il12a*	*Cxcl12*	*Was*
Il10	*Bmp6*	*H2-T24*	*Cd1d2*	*Clec4e*	
Sbspon	*Hfe*	*H2-T23*	*Il7*	*Cd4*	
Prg4	*Cxcl14*	*H2-T22*	*Il2*	*Mill1*	
Fasl	*Il9*	*Gm7030*	*Il21*	*Mill2*	
Xcl1	*Bmpr1a*	*H2-Bl*	*Cd1d1*	*Igf1r*	
Fcgr2b	*Tnfsf11*	*H2-T10*	*Ifi44l*	*Mylpf*	
Cd24a	*C6*	*H2-T3*	*Ccl27b*	*Psg17*	
Zfr2	*C7*	*H2-M10.2*	*Gm13304*	*Cebpg*	
9230019H11Rik	*Ptger4*	*H2-M10.1*	*Tnfsf15*	*Fcgrt*	
Enpp1	*Enpp2*	*H2-M10.3*	*Tnfsf8*	*Lat*	
Enpp3	*Endou*	*H2-M10.4*	*C8a*	*Ccl25*	
Susd2	*Cblb*	*H2-M9*	*Tinagl1*	*Tnfsf13b*	
Osm	*Vpreb1*	*H2-M1*	*Tnfrsf1b*	*March1*	
Lif	*Nrros*	*H2-M5*	*Cxcl5*	*Ccl22*	
Il5	*Ccr6*	*H2-M2*	*Cxcl3*	*Cx3cl1*	
Vtn	*H2-Oa*	*Cd70*	*Cxcl15*	*Ccl17*	
Ccl7	*H2-DMb2*	*Tnfsf14*	*Cxcl1*	*Irf8*	
Ccl11	*H2-Ob*	*Colec12*	*Cxcl2*	*Il15*	
Ccl12	*H2-Ab1*	*Fth1*	*Cxcl13*	*Il18*	
Ccl8	*H2-Eb1*	*Cd274*	*Oasl2*	*Tlr9*	
Ccl4	*H2-Eb2*	*Nkx2-3*	*Oas1b*	*Ccr8*	
Csf3	*Ltb*	*Ms4a2*	*Oas1f*	*Ccr9*	
Tgtp1	*H2-D1*	*Lax1*	*Oas1h*	*Ccr2*	

Il13	*H2-Q1*	*Il1f8*	*Oas1d*	*Cxcr5*	
Csf2	*H2-Q2*	*Il1f6*	*Azgp1*	*Smad3*	
Il3	*H2-Q4*	*Prg2*	*Cxcl9*	*Smad6*	
Tnfsf12Tnfsf13	*H2-Q6*	*Prg3*	*Gbp6*	*Tinag*	
Tnfaip1	*H2-Q10*	*Traf6*	*Tgfbr3*	*Ccr4*	

Supplementary Table 7. Differentially regulated genes of immunogenic profiles of SMA-497 and GL-261 mouse glioma cell lines, as defined by Gene Ontology classification schemes.

Immune response-related genes up-regulated in SMA-497	**Immune response-related genes up-regulated in GL-261**	**Immune response-related genes down-regulated in GL-261**
Smad6; Map3k14 Ccl9; Bmpr1a; Igf1r; Bmp6; Ccl8; Cd24a; Il15; Enpp2; Cx3cl1; Fcgrt; Ccl17; Cxcl1; Il7; Cxcl12 Cxcl5; Cd1d1; thbs1	*Oasl2; Oas1g; Tgtp1 Gbp6; Oas1b; Enpp1 Ccl5; Cd274; H2−Bl Lst1; Mill2; Nrros Tnfsf10; Bpi; Psg17 C7; H2−DMb2; Enpp3 Ccl25; Tnfsf9; H2−Q4 H2−K1; Oas3; H2−T23 Azgp1; Tinagl1; Il18*	*Smad3; Tnfrsf1b; Eda Lif; Cblb; Tgfbr3 Colec12; ccl7 ; Cx3cl1; Fcgrt; Ccl17 ; Cxcl1; Il7; Cxcl12 ; Cxcl5; cd1d1*

Supplementary materials and methods

Cell lines

The cells have been characterized extensively in our laboratory [1] and are commonly cultured as adherent monolayers in Dulbecco`s modified Eagle medium (DMEM) (Gibco, Invitrogen AG, Basel, Switzerland) supplemented with 10% heat-inactivated fetal calf serum (FCS) (Biochrom KG, Zug, Switzerland) and 2 mM glutamine (Biochrom KG) (DM medium). Hypoxia treatment was done in a hypoxia chamber at 1% O_2 atmosphere.

Viability and clonogenicity assays

Clonogenicity was assessed as previously described [2]. Briefly, 100 cells per well were seeded in 96-well plates, allowed to adhere overnight, and treated for 24 h with either LY2157299 (Eli Lilly & Co, 1 µM), cediranib (AstraZeneca, 100 nM) or B20 (Genentech, 100 µg/ml) in fresh medium followed by an observation period for 10 to 14 days in serum-containing medium. Cell density was assessed by counting crystal violet stained colonies.

Real-time PCR (RT-PCR) and primers

The conditions for RT-PCR were 40 cycles, 95°C/15s, 60°C/30s, 72°C/30s. Relative quantification of gene expression was obtained by comparison of cycle threshold values. Hypoxanthine phosphoribosyltransferase 1 (*HPRT1*) was used as a housekeeping gene and specific target gene expression was normalized to *HPRT1* and calculated with the ΔC_T-method for relative quantification with respect to primer efficiency calculated by the standard curve method. The following mouse-specific primers were used: *HPRT1* (forward 5'-TTGCTGACCTGCTGGATTAC-3', reverse 5'-TTTATGTCCCCCGTTGACTG-3'), *VEGF* (forward 5'-CACGACAGAAGGAGAGCAGA-3', reverse 5'-GGGCTTCATCGTTACAGCAG-3'), *VEGFR1* (forward 5'-

AGAGGAGGATGAGGGTGTCT-3', reverse 5'-GGGAACTTCATCTGGGTCCA-3'),*VEGFR2* (forward 5'-GCTCCTGACTACACTACCCC-3', reverse 5'-AGGAAACAGGTGAGGTAGGC-3'), *TGF-β_1* (forward 5′-TGGAGCAACATGTGGAACTC-3′, reverse 5′- GTCAGCAGCCGGTTACCA-3′), *TGF-β_2*, (forward 5′-GCCCACTTTCTACAGACCCT -3′, reverse 5′-CCTTGCTATCGATGTAGCGC-3′), *ALK-5* (forward 5'- TGGGACTTGCTGTGAGACAT-3', reverse 5'- CCACCAATAGAACAGCGTCG-3') and *TGF-βR2* (forward 5'-CTGTTGCCTGTGTGACTTCG-3', reverse 5'-AACGACTCCACGTTTTC-3') (all Microsynth, Balgach, Switzerland).

Immunoblot analyses

For immunoblot analysis, whole cell lysates were prepared using RIPA lysis buffer containing 1% NP-40, 0.5% sodium deoxycholate, 50 mM Tris/HCl pH 8.0, 150 mM NaCl, 5 mM EDTA pH 8.0, 0.1% SDS in Milli-Q water supplemented with 2 µg/mL aprotinin, 10 µg/mL leupeptin, 100 µg/mL phenylmethylsulfonyl fluoride, phosphatase inhibitor cocktails 2 and 3 (Sigma Aldrich, St. Louis, MO). Protein levels were determined using BCA Protein Assay Kit (Pierce/Thermo Fisher, Madison, WI). After SDS-PAGE (8 – 12 % acrylamide gels) under reducing conditions with loading of equal amounts of proteins, proteins were transferred to nitrocellulose membranes (Biorad, Hercules, CA), blocked in Tris-buffered saline containing 5% skim milk and 0.1% Tween 20 and incubated with the following antibodies at concentrations recommended by the manufacturers: anti-VEGFR1 (R&D Systems, AF471), anti-VEGFR2 (Cell Signaling, Leiden, Netherlands, #2479), anti-pSMAD2 (Cell Signaling, #3108), anti-ALK-5 (Santa Cruz Biotechnology, Inc., Dallas, TX, sc-9048), anti-TGFβR2 (R&D Systems, AF532), anti-β-actin (Santa Cruz Biotechnology, Inc., sc-1616). Visualization of protein bands was accomplished using horseradish peroxidase (HRP)-coupled secondary antibodies (Santa Cruz) and enhanced chemoluminescence (Pierce/Thermo

Fisher, Madison, WI). For quantitative correlation analyses of baseline expression of total and phosphorylated proteins, band intensity was analyzed via densitometry using ImageJ software (http://imagej.nih.gov/ij/index.html, Open Source).

Enzyme-linked immunosorbent assay (ELISA)

Supernatants were collected from subconfluent glioma cell cultures after the indicated time periods. Treatments were performed in SFM for the indicated time periods. Cellular debris was removed by centrifugation and supernatants were concentrated using 3K-Amicon® Ultra-4 Centrifugal Filter Units (Millipore AG, Zug, Switzerland). ELISA kits for murine VEGF (VEGF, eBiosciences, San Diego, BM5619/2), murine TGF-β_1 (eBiosciences, BMS608/4) and TGF-β_2 (R&D, MB200) were used. Results were normalized to the cell numbers at the time of harvesting.

Animal studies

Following anesthesia, a burr hole was drilled in the skull 2 mm lateral to the bregma. The needle of a Hamilton syringe (Hamilton, Darmstadt, Germany) was introduced to a depth of 3 mm. A volume of 2 µl of a single cell suspension in PBS was slowly injected into the right striatum. In VM/Dk mice 5 x 10^3 SMA glioma cells were implanted, whereas in C57Bl/6 mice 2 x 10^4 GL-261 cells were implanted (n=10 per group). Systemic treatment was performed by i.p. injections of B20 (5 mg/kg body weight twice weekly) or the solvent PBS, or by oral gavage delivering the TGF-βR1 inhibitor LY2157299 (150 mg/kg weight/daily) or the solvent (1% w/v HEC/0.25% v/v Tween 80/ 0.05 v/v Antifoam 1510-US in H_2O). The mice were observed daily and euthanized when developing neurological symptoms or at defined time points for histological analysis as indicated. Three mice per group were commonly euthanized using a pre-randomization list when any mouse in the experiment became symptomatic (early-stage) in order to perform histological studies to assess tumor

growth at an early stage. The remaining 7 mice were euthanized when displaying neurological symptoms to obtain survival or histological data (end-stage). Where indicated, mice brains were explanted for snap-frozen samples. All brains were collected upon euthanization, embedded in cryomoulds in Shandon Cytochrome yellow (Thermo Scientific, Waltham, MA) and frozen in liquid nitrogen. Tumor incidences and sizes were determined using hematoxylin and eosin stainings of 8 µm thick cryosections cut using a Microm HM560 (Microchom HM560, Thermo Scientific). Each experiment was performed at least twice.

Immunohistochemical analysis

Cryosections were fixed in 4% formalin, acetone or methanol/acetone for 10 min, air-dried, pretreated with 0.3-3% H_2O_2 and blocked in 10% rabbit or donkey serum or blocking solution (Candor Biosciences, Wangen, Germany). After blocking, the primary antibodies were applied for 1 h at 37°C or overnight at 4°C. Primary antibodies were polyclonal goat anti-CA IX (R&D Systems, AF2344, 1:50), monoclonal rat anti-CD4 (BD Pharmingen, 553727, 1:100), monoclonal rat anti-CD8a (BD Pharmingen, BD550281, 1:50), polyclonal rabbit anti-CD11b (Abcam, Cambridge, UK, ab75476, 1:400), monoclonal rat anti-CD31 (BD Pharmingen, Allschwil, Switzerland, BD550274, 1:50), monoclonal rat anti-CD45 (Biolegend, San Diego, CA, 103102, 1:1000), monoclonal rabbit anti-Ki-67 (Epitomics, Burlingame, CA) and monoclonal rabbit anti-pSMAD2 (Cell Signaling, 3108, 1:1000). Biotinylated secondary antibodies, streptavidin and 3,3′-diaminobenzidine (DAB) were obtained from Dako (Baar, Switzerland). Histofine Simple Stain Mouse MAX PO secondary-labelled antibody system was obtained from Nichirei (Tokyo, Japan). Secondary antibodies were incubated for 30 min at room temperature. The antigen antibody conjugates were then detected by staining with DAB (Dako) for 1-3 min. The nuclei were stained using hematoxylin for up to 4 min, washed in water and dehydrated twice in 96% ethanol, then twice in 100% ethanol and three times in xylol before mounting onto coverslips using Eukitt

mounting medium (Sigma Aldrich). Quantification of immunohistological stainings was obtained from 4 regions of interest (ROI) from 3 tumors per group. Within tumor tissue, percentages of CD11b- and CD45-positive cells of all nucleated cells were determined, microvessel density (MVD) was calculated by counting $CD31^+$ capillaries, and infiltrating CD4 and CD8a positive cells per ROI were counted. Quantification of pSMAD2-positive cells was performed by H scoring in four randomly selected, different microscopic fields of independent hotspots (tumor margin) and tumor centers on the basis of both the percentage of positive tumor nuclei and staining intensity in tumors [3]. In brief, to obtain scores, staining intensity is scored as absent (0), mild (1), moderate (2) or strong (3) expression. The staining intensity value is multiplied by the percentage of cells showing each grade of positivity, thus, the maximum H score is 300 [4,5]. The surface detection function within the Image J software was used for the quantification of CD11b-, CD45- and Ki-67-positive cells and for Carbonic anidrase IX (CA IX)-positive areas. Tumor volumes were calculated using an approximation based on ellipsoid geometric primitive [6].

Immunofluorescence microscopy

Immunofluorescence studies were carried out on cryosections of tumor-bearing mouse brains and on paraffin-embedded sections from 14 paired surgical glioma samples from patients that were exposed to salvage therapy regimens without or with bevacizumab in between two surgical interventions. Briefly, formalin-fixed paraffin-embedded (FFPE) tumor tissue samples were deparaffinized with xylene for 30 min and rehydrated. The following antibodies were applied overnight at 4°C: polyclonal anti-CA IX (R&D Systems), monoclonal anti-CD31 (BD Pharmingen), monoclonal pSMAD2 (Cell Signaling), monoclonal rat anti-VEGFR1 (Biolegend, 136402, 1:50) and monoclonal rabbit anti-VEGFR2 (Cell Signaling, 2479, 1:200). Binding specificity was controlled by IgG isotype control (Jackson Immunoresearch, West Grove, PA). For visualization, Alexa Fluor 488 goat anti-rabbit IgG

(Life Technologies, Zug, Switzerland, A-11008) or Alexa Fluor 594 donkey anti-rat IgG (Life Technologies, A-21209) were applied. All sections were mounted in Dako Fluorescent Mounting Medium (Dako). DNA was stained with 4',6-diamidino-2-phenylindole (DAPI). Pictures were taken with a ×63 oil immersion objective (1.4 numerical aperture; Leica Microsystems, Heerbrugg, Switzerland). A CLSM Leica SP5 microscope (Leica Microsystems) attached to a diode and an argon laser was used to provide excitation at 405 nm, 488 nm and 561 nm wavelengths. The emitted fluorescence light was detected via three adjustable photomultiplier detectors. Per brain section, two single images from randomly selected ROI were recorded and included in the quantification. The surface detection function within the Bitplane Imaris (Bitplane) software [7] was used for quantification of pSMAD2 staining.

Analysis of gene expression data

The microarray data have been presented previously [1]. Raw microarray data were calibrated and summarized using the hook method including quantile-normalization [8-10]. The expression value of each gene was transformed into log10-scale and centered with respect to its mean value averaged over all samples investigated [11]. Differential expression analysis was performed using pairwise comparisons of sample classes and by applying a shrinkage t-score combined with false discovery rate multiple test correction for judgement of significance [12]. For functional analysis we applied gene set enrichment analysis based on predefined gene sets taken from the literature, from gene ontology classification schemes, or from gene lists determined in this study. All methods were implemented in the program opoSOM that was used for all analyses [13].

Search Tool for the Retrieval of Interacting Genes/Proteins (STRING) analysis

Functional gene interactions were analysed with the STRING Version 10 at http://string-db.org [14]. High confidence settings were applied, integrating combined scores higher than 0.700. Cluster analysis was performed by application of the Markov Cluster algorithm (MCL).

Statistical analyses

All *in vitro* data are representative of experiments performed in three independent experiments with similar results. Statistical significance was assessed using either two-sided paired or unpaired Student's *t*-test or one-way ANOVA with Tukey's post hoc test for multiple analysis. Quantitative data are represented as mean ± standard deviation (SD) for *in vitro* or standard error of the mean (SEM) for *in vivo* experiments. A p value below 0.01 was considered significant. Kaplan Meier survival curves generated from the animal studies were analyzed using the log-rank test or the Gehan-Breslow-Wilcoxon test. A p value below 0.05 was considered significant. All statistical analyses were performed using Prism 5 (GraphPad Software, La Jolla, CA).

Supplementary References

1. Ahmad M, Frei K, Willscher E, et al. How stemlike are sphere cultures from long-term cancer cell lines? Lessons from mouse glioma models. *Journal of neuropathology and experimental neurology.* 2014; 73(11):1062-1077.

2. Happold C, Roth P, Silginer M, et al. Interferon-beta induces loss of spherogenicity and overcomes therapy resistance of glioblastoma stem cells. *Molecular cancer therapeutics.* 2014; 13(4):948-961.

3. Frei K, Gramatzki D, Tritschler I, et al. Transforming growth factor-beta pathway activity in glioblastoma. *Oncotarget.* 2015; 6(8):5963-5977.

4. Kraus JA, Dabbs DJ, Beriwal S, Bhargava R. Semi-quantitative immunohistochemical assay versus oncotype DX((R)) qRT-PCR assay for estrogen and progesterone receptors: an independent quality assurance study. *Modern pathology : an official journal of the United States and Canadian Academy of Pathology, Inc.* 2012; 25(6):869-876.

5. Kinsel LB, Szabo E, Greene GL, Konrath J, Leight GS, McCarty KS, Jr. Immunocytochemical analysis of estrogen receptors as a predictor of prognosis in breast cancer patients: comparison with quantitative biochemical methods. *Cancer research.* 1989; 49(4):1052-1056.

6. Schmidt KF, Ziu M, Schmidt NO, et al. Volume reconstruction techniques improve the correlation between histological and in vivo tumor volume measurements in mouse models of human gliomas. *Journal of neuro-oncology.* 2004; 68(3):207-215.

7. Roth P, Silginer M, Goodman SL, et al. Integrin control of the transforming growth factor-beta pathway in glioblastoma. *Brain : a journal of neurology.* 2013; 136(Pt 2):564-576.

8. Binder H, Krohn K, Preibisch S. "Hook"-calibration of GeneChip-microarrays: chip characteristics and expression measures. *Algorithms for molecular biology : AMB.* 2008; 3:11.

9. Binder H, Preibisch S. "Hook"-calibration of GeneChip-microarrays: theory and algorithm. *Algorithms for molecular biology : AMB.* 2008; 3:12.

10. Irizarry RA, Hobbs B, Collin F, et al. Exploration, normalization, and summaries of high density oligonucleotide array probe level data. *Biostatistics.* 2003; 4(2):249-264.

11. Wirth H, Loffler M, von Bergen M, Binder H. Expression cartography of human tissues using self organizing maps. *BMC bioinformatics.* 2011; 12:306.

12. Wirth H, von Bergen M, Binder H. Mining SOM expression portraits: feature selection and integrating concepts of molecular function. *BioData mining.* 2012; 5(1):18.

13. Loffler-Wirth H, Kalcher M, Binder H. oposSOM: R-package for high-dimensional portraying of genome-wide expression landscapes on Bioconductor. *Bioinformatics.* 2015.

14. Franceschini A, Szklarczyk D, Frankild S, et al. STRING v9.1: protein-protein interaction networks, with increased coverage and integration. *Nucleic acids research.* 2013; 41(Database issue):D808-815.

Supplementary Fig. S1 VEGF and TGF-β pathway ligand and receptor expression in experimental mouse gliomas in vivo. A-C Explanted SMA-497, SMA-540, SMA-560 or GL-261 mouse tumors (T) were studied for *VEGF* and *VEGFR1,2* mRNA expression. MC and normal brain tissue of the respective mouse strain (VM/Dk or C57BL/6) served as references. (A) *VEGF*, (B) *VEGFR1*, (C) *VEGFR2*. Three ex vivo tissue samples per group were analysed. Data are expressed as mean and SD (*p<0.05, **p<0.01, unpaired student t-test, T versus MC). D,E, Immunofluorescent stainings of VEGFR2 in mouse glioma tissues (D) and normal brain tissue (E) were performed (size bar: 20 μM). F-I Explanted tumors (T) were studied for *TGF-β1/2*, *TGF-βR2* and *ALK-5* mRNA expression. MC and normal brain tissue of the respective mouse strain (VM/Dk or C57BL/6) served as references. (F) *TGF-β1*, (G) *TGF-β2*, (H) *TGF-βR2*, (I) *ALK-5*. Three ex vivo tissue samples per group were analysed (*p<0.05, **p<0.01, ***p<0.001, unpaired student t-test, T versus MC). Each experimental and control group contained 3 mice for histological examination and 3 animals for expression analysis. Each experiment was performed at least twice

Supplementary Fig. S2 VEGF and TGF-β signaling in mouse glioma cells in vitro. A, pVEGFR1,2 levels after VEGF stimulation (400 ng/ml,5 min) were assessed by immunoblot. B, pSMAD2 levels of cells either treated with 1 μM LY2157299 or 2 ng/ml TGF-β2 or both (SMA-540, SMA-560 for 3 h, SMA-497, GL-261 for 24 h) were analyzed. C, pSMAD2 levels were assessed under normoxic or hypoxic conditions (24 h, 1% O2). Values of densitometric analysis of pVEGFR and pSMAD2 protein levels, relative to β-actin, are shown below the immunoblot panels. D,E, Mouse glioma cells were exposed to LY2157299 (24 h, 1 μM), cediranib (24 h, 100 nM) or B20 (24 h, 100 μg/ml). D, Viability was assessed by trypan blue exclusion assay. E, Clonogenic survival was assessed by measuring cell density via crystal violet staining. Quantitative data are expressed as mean and SEM (***p<0.001, one-

way ANOVA followed by Tukey's post hoc test, confidence interval 99%, LY2157299 or cediranib versus DMSO)

Supplementary Fig. S3 Differential effects of murinized bevacizumab on angiogenesis, leukocyte infiltration and growth of murine gliomas. Syngeneic mice intracranially implanted with SMA-497, SMA-540, SMA-560 or GL-261 cells were treated twice weekly with 5 mg/kg B20 or PBS from day 7 on. a-e Brain sections from animals sacrificed when the first mice became symptomatic were stained with H&E (A) or by immunohistochemistry for Ki-67 (B), CD31 (C), CA IX (D) or pSMAD2 (E). F, Vessel density and tumor hypoxia in untreated murine SMA-497 or SMA-560 gliomas were assessed by immunofluorescent stainings for CA IX (green) and CD31 (red), using nuclear counterstaining with DAPI (blue). Merged images are provided as indicated in right images of each row. G, pSMAD2 levels were determined in tumor cells and leukocytes upon B20 treatment in the SMA-560 model in vivo. Immunofluorescent stainings were performed for pSMAD2 (green) and CD45 (red), again using DAPI as a counterstain. Merged images are provided as indicated in right images of each row. Size bars correspond to 100 μM (A,C,D) and 50 μM (B,E-G). Each experimental and control group contained 3 mice for histological examination. Each experiment was performed at least twice. H,I Gene cluster analysis. Functional interactions between genes up-regulated in the angiogenic profiles of SMA-497 (H) and GL-261 (I, top) or down-regulated in GL-261 (I, bottom) were analyzed in Affymetrix micro-array based gene expression profiling by STRING analysis. Interactions with high confidence score of 0.700 were integrated to the interactome. Clusters were determined by MCL algorithm and presented with different node colors. Inter-cluster edges are represented by dashed-lines

Supplementary Fig. S4 Differential effects of LY2157299 on the growth of murine gliomas. Mice intracranially implanted with SMA-497, SMA-540, SMA-560 or GL-261 cells were treated daily with LY2157299 at 150 mg/kg or control solvent from day 7 on. A-C Brain sections from animals sacrificed when the first mice became symptomatic. A H&E. B Immunohistochemical stainings of pSMAD2 (top) and protein levels determined by immunoblot (bottom). Values of densitometric analysis of pSMAD2 protein levels, relative to β-actin, are shown below the immunoblot panels. (C) CD31. Size bars within images correspond to 50 μm (B) and 100 μm (A,C). Each experimental and control group contained 3 mice for histological examination. Each experiment was performed at least twice. D,E Gene cluster analysis. Functional interactions between genes up-regulated in immune response pathways in SMA-497 (D) and GL-261 (E,top) or down-regulated in GL-261 (E,bottom/) were analyzed by Affymetrix micro-array based gene expression profiling using STRING analysis. Interactions with high confidence score of 0.700 were integrated to the interactome. Clusters were determined by MCL algorithm and presented with different node colors. Inter-cluster edges are represented by dashed-lines

Supplementary Fig. S5 Modulation of the VEGF and TGF-β signaling pathway by VEGF in vitro. A,B Modulation of TGF-β1 (A) or TGF-β2 (B) mRNA (left) expression was determined by RT-PCR 24 h after exposure to VEGF (400 ng/ml), cediranib (100 nM) or B20 (100 μg/ml). Protein levels (right) were detected in corresponding supernatants by ELISA. Data are expressed as mean and SD (n=3) (one-way ANOVA followed by Tukey's post hoc test, confidence interval 99%). C, pSMAD2 levels were assessed by immunoblot. Values of densitometric analysis of pSMAD2 protein levels relative to β-actin are shown below the immunoblot panels. D,E The cells were treated with TGF-β2 (2 ng/ml) or LY2157299 (1 μM) or both for 24 h. *VEGF* mRNA expression was assessed by RT-PCR (D). In parallel, VEGF

protein levels were determined by ELISA (E). F,G VEGFR1/2 mRNA (left) and protein (right) levels were assessed by immunoblot. mRNA and ELISA data are expressed as mean and SD (n=3) (***$p<0.001$, one-way ANOVA followed by Tukey's post hoc test confidence interval 99%, treated versus SFM, ++$p<0.01$, +++$p<0.001$, LY2157299 + TGF-β2 versus TGF-β2, ##$p<0.01$, ###$p<0.001$, hypoxia versus SFM). Values of densitometric analysis of VEGFR protein levels, relative to β-actin, are shown below the immunoblot panels in F and G

Supplementary Fig. S6 Effect of combined B20 and LY2157299 treatment in SMA-497 and GL-261 syngeneic models in vivo. Syngeneic mice intracranially implanted with SMA-497 or GL-261 cells were treated twice weekly with 5 mg/kg B20 or daily with 150 mg/kg LY2157299 or corresponding solvents or both. A-L Brain sections from animals sacrificed when the first mice became symptomatic (early-stage) (A-D) and at the time point when each specific mouse developed neurological symptoms (end-stage) (E-L) were examined. Morphology was assessed by H&E staining (A,E). Brains were immunohistochemically stained for CD31 (B,F), pSMAD2 (C,G), CA IX (D,H). I-L Staining of tumor sections to visualize vessel normalization was performed with DAPI (I, blue), CD31 (J, red) and ZO-1 (K, green). Merged images are shown in (L). Size bars correspond to 100 μm (A,B,D-F,H), 50 μm (C,G) or 10 μm (I,L). Each experimental and control group contained 3 mice for histological examination. Each experiment was performed at least twice

Supplementary Fig. S7 Effect of combined B20 and LY2157299 treatment in SMA-497 and GL-261 syngeneic models in vivo. Syngeneic mice intracranially implanted with SMA-497 or GL-261 cells were treated twice weekly with 5 mg/kg B20 or daily with 150 mg/kg LY2157299 or corresponding solvents or both. A-H Brain sections from animals sacrificed

when the first mice became symptomatic (early-stage) (A-D) and at the time point when each specific mouse developed neurological symptoms (end-stage) (E-H) were examined. Brains were immunohistochemically stained for CD45 (A,E), CD4 (B,F), CD8 (C,G) or CD11b (D,H). Size bars correspond to 50 μm. Each experimental and control group contained 3 mice for histological examination. Each experiment was performed at least twice.

Supplementary Fig. S8 pSMAD2 levels in bevacizumab-treated patients. pSMAD2 levels were assessed by immunofluorescence microscopy in primary and recurrent tumor tissue of patients treated with non-bevacizumab regimens (A) or bevacizumab-containing regimens (B). Size bars correspond to 20 μM. Quantification of fluorescent images of the two cohorts are provided in C and D. E,F Vessel density scores. Data are expressed as mean and SEM ($^{*}p<0.05$, paired student t-test, primary versus recurrent).